Eur. Phys. J. C 8, 3–21 (1999)
DOI 10.1007/s100529901080

THE EUROPEAN PHYSICAL JOURNAL C


# Measurement of the Michel parameters in leptonic tau decays

The OPAL Collaboration

K. Ackerstaff[8], G. Alexander[23], J. Allison[16], N. Altekamp[5], K.J. Anderson[9], S. Anderson[12], S. Arcelli[2], S. Asai[24], S.F. Ashby[1], D. Axen[29], G. Azuelos[18,a], A.H. Ball[17], E. Barberio[8], R.J. Barlow[16], R. Bartoldus[3], J.R. Batley[5], S. Baumann[3], J. Bechtluft[14], T. Behnke[8], K.W. Bell[20], G. Bella[23], S. Bentvelsen[8], S. Bethke[14], S. Betts[15], O. Biebel[14], A. Biguzzi[5], S.D. Bird[16], V. Blobel[27], I.J. Bloodworth[1], M. Bobinski[10], P. Bock[11], J. Böhme[14], M. Boutemeur[34], S. Braibant[8], P. Bright-Thomas[1], R.M. Brown[20], H.J. Burckhart[8], C. Burgard[8], R. Bürgin[10], P. Capiluppi[2], R.K. Carnegie[6], A.A. Carter[13], J.R. Carter[5], C.Y. Chang[17], D.G. Charlton[1,b], D. Chrisman[4], C. Ciocca[2], P.E.L. Clarke[15], E. Clay[15], I. Cohen[23], J.E. Conboy[15], O.C. Cooke[8], C. Couyoumtzelis[13], R.L. Coxe[9], M. Cuffiani[2], S. Dado[22], G.M. Dallavalle[2], R. Davis[30], S. De Jong[12], L.A. del Pozo[4], A. de Roeck[8], K. Desch[8], B. Dienes[33,d], M.S. Dixit[7], M. Doucet[18], J. Dubbert[34], E. Duchovni[26], G. Duckeck[34], I.P. Duerdoth[16], D. Eatough[16], P.G. Estabrooks[6], E. Etzion[23], H.G. Evans[9], F. Fabbri[2], A. Fanfani[2], M. Fanti[2], A.A. Faust[30], F. Fiedler[27], M. Fierro[2], H.M. Fischer[3], I. Fleck[8], R. Folman[26], A. Fürtjes[8], D.I. Futyan[16], P. Gagnon[7], J.W. Gary[4], J. Gascon[18], S.M. Gascon-Shotkin[17], C. Geich-Gimbel[3], T. Geralis[20], G. Giacomelli[2], P. Giacomelli[2], V. Gibson[5], W.R. Gibson[13], D.M. Gingrich[30,a], D. Glenzinski[9], J. Goldberg[22], W. Gorn[4], C. Grandi[2], E. Gross[26], J. Grunhaus[23], M. Gruwé[27], G.G. Hanson[12], M. Hansroul[8], M. Hapke[13], C.K. Hargrove[7], C. Hartmann[3], M. Hauschild[8], C.M. Hawkes[5], R. Hawkings[27], R.J. Hemingway[6], M. Herndon[17], G. Herten[10], R.D. Heuer[8], M.D. Hildreth[8], J.C. Hill[5], S.J. Hillier[1], P.R. Hobson[25], A. Hocker[9], R.J. Homer[1], A.K. Honma[28,a], D. Horváth[32,c], K.R. Hossain[30], R. Howard[29], P. Hüntemeyer[27], P. Igo-Kemenes[11], D.C. Imrie[25], K. Ishii[24], F.R. Jacob[20], A. Jawahery[17], H. Jeremie[18], M. Jimack[1], A. Joly[18], C.R. Jones[5], P. Jovanovic[1], T.R. Junk[8], D. Karlen[6], V. Kartvelishvili[16], K. Kawagoe[24], T. Kawamoto[24], P.I. Kayal[30], R.K. Keeler[28], R.G. Kellogg[17], B.W. Kennedy[20], A. Klier[26], S. Kluth[8], T. Kobayashi[24], M. Kobel[3,e], D.S. Koetke[6], T.P. Kokott[3], M. Kolrep[10], S. Komamiya[24], R.V. Kowalewski[28], T. Kress[11], P. Krieger[6], J. von Krogh[11], P. Kyberd[13], G.D. Lafferty[16], D. Lanske[14], J. Lauber[15], S.R. Lautenschlager[31], I. Lawson[28], J.G. Layter[4], D. Lazic[22], A.M. Lee[31], E. Lefebvre[18], D. Lellouch[26], J. Letts[12], L. Levinson[26], R. Liebisch[11], B. List[8], C. Littlewood[5], A.W. Lloyd[1], S.L. Lloyd[13], F.K. Loebinger[16], G.D. Long[28], M.J. Losty[7], J. Ludwig[10], D. Liu[12], A. Macchiolo[2], A. Macpherson[30], M. Mannelli[8], S. Marcellini[2], C. Markopoulos[13], A.J. Martin[13], J.P. Martin[18], G. Martinez[17], T. Mashimo[24], P. Mättig[26], W.J. McDonald[30], J. McKenna[29], E.A. Mckigney[15], T.J. McMahon[1], R.A. McPherson[28], F. Meijers[8], S. Menke[3], F.S. Merritt[9], H. Mes[7], J. Meyer[27], A. Michelini[2], S. Mihara[24], G. Mikenberg[26], D.J. Miller[15], R. Mir[26], W. Mohr[10], A. Montanari[2], T. Mori[24], K. Nagai[26], I. Nakamura[24], H.A. Neal[12], B. Nellen[3], R. Nisius[8], S.W. O'Neale[1], F.G. Oakham[7], F. Odorici[2], H.O. Ogren[12], M.J. Oreglia[9], S. Orito[24], J. Pálinkás[33,d], G. Pásztor[32], J.R. Pater[16], G.N. Patrick[20], J. Patt[10], R. Perez-Ochoa[8], S. Petzold[27], P. Pfeifenschneider[14], J.E. Pilcher[9], J. Pinfold[30], D.E. Plane[8], P. Poffenberger[28], B. Poli[2], J. Polok[8], M. Przybycień[8], C. Rembser[8], H. Rick[8], S. Robertson[28], S.A. Robins[22], N. Rodning[30], J.M. Roney[28], K. Roscoe[16], A.M. Rossi[2], Y. Rozen[22], K. Runge[10], O. Runolfsson[8], D.R. Rust[12], K. Sachs[10], T. Saeki[24], O. Sahr[34], W.M. Sang[25], E.K.G. Sarkisyan[23], C. Sbarra[29], A.D. Schaile[34], O. Schaile[34], F. Scharf[3], P. Scharff-Hansen[8], J. Schieck[11], B. Schmitt[8], S. Schmitt[11], A. Schöning[8], T. Schorner[34], M. Schröder[8], M. Schumacher[3], C. Schwick[8], W.G. Scott[20], R. Seuster[14], T.G. Shears[8], B.C. Shen[4], C.H. Shepherd-Themistocleous[8], P. Sherwood[15], G.P. Siroli[2], A. Sittler[27], A. Skuja[17], A.M. Smith[8], G.A. Snow[17], R. Sobie[28], S. Söldner-Rembold[10], M. Sproston[20], A. Stahl[3], K. Stephens[16], J. Steuerer[27], K. Stoll[10], D. Strom[19], R. Ströhmer[34], R. Tafirout[18], S.D. Talbot[1], S. Tanaka[24], P. Taras[18], S. Tarem[22], R. Teuscher[8], M. Thiergen[10], M.A. Thomson[8], E. von Törne[3], E. Torrence[8], S. Towers[6], I. Trigger[18], Z. Trócsányi[33], E. Tsur[23], A.S. Turcot[9], M.F. Turner-Watson[8], R. Van Kooten[12], P. Vannerem[10], M. Verzocchi[10], P. Vikas[18], H. Voss[3], F. Wäckerle[10], A. Wagner[27], C.P. Ward[5], D.R. Ward[5], P.M. Watkins[1], A.T. Watson[1], N.K. Watson[1], P.S. Wells[8], N. Wermes[3], J.S. White[28], G.W. Wilson[14], J.A. Wilson[1], T.R. Wyatt[16], S. Yamashita[24], G. Yekutieli[26], V. Zacek[18], D. Zer-Zion[8]

[1] School of Physics and Astronomy, University of Birmingham, Birmingham B15 2TT, UK
[2] Dipartimento di Fisica dell' Università di Bologna and INFN, I-40126 Bologna, Italy
[3] Physikalisches Institut, Universität Bonn, D-53115 Bonn, Germany
[4] Department of Physics, University of California, Riverside CA 92521, USA
[5] Cavendish Laboratory, Cambridge CB3 0HE, UK
[6] Ottawa-Carleton Institute for Physics, Department of Physics, Carleton University, Ottawa, Ontario K1S 5B6, Canada

[7] Centre for Research in Particle Physics, Carleton University, Ottawa, Ontario K1S 5B6, Canada
[8] CERN, European Organisation for Particle Physics, CH-1211 Geneva 23, Switzerland
[9] Enrico Fermi Institute and Department of Physics, University of Chicago, Chicago IL 60637, USA
[10] Fakultät für Physik, Albert Ludwigs Universität, D-79104 Freiburg, Germany
[11] Physikalisches Institut, Universität Heidelberg, D-69120 Heidelberg, Germany
[12] Indiana University, Department of Physics, Swain Hall West 117, Bloomington IN 47405, USA
[13] Queen Mary and Westfield College, University of London, London E1 4NS, UK
[14] Technische Hochschule Aachen, III Physikalisches Institut, Sommerfeldstrasse 26-28, D-52056 Aachen, Germany
[15] University College London, London WC1E 6BT, UK
[16] Department of Physics, Schuster Laboratory, The University, Manchester M13 9PL, UK
[17] Department of Physics, University of Maryland, College Park, MD 20742, USA
[18] Laboratoire de Physique Nucléaire, Université de Montréal, Montréal, Quebec H3C 3J7, Canada
[19] University of Oregon, Department of Physics, Eugene OR 97403, USA
[20] Rutherford Appleton Laboratory, Chilton, Didcot, Oxfordshire OX11 0QX, UK
[22] Department of Physics, Technion-Israel Institute of Technology, Haifa 32000, Israel
[23] Department of Physics and Astronomy, Tel Aviv University, Tel Aviv 69978, Israel
[24] International Centre for Elementary Particle Physics and Department of Physics, University of Tokyo, Tokyo 113, and Kobe University, Kobe 657, Japan
[25] Institute of Physical and Environmental Sciences, Brunel University, Uxbridge, Middlesex UB8 3PH, UK
[26] Particle Physics Department, Weizmann Institute of Science, Rehovot 76100, Israel
[27] Universität Hamburg/DESY, II Institut für Experimental Physik, Notkestrasse 85, D-22607 Hamburg, Germany
[28] University of Victoria, Department of Physics, P O Box 3055, Victoria BC V8W 3P6, Canada
[29] University of British Columbia, Department of Physics, Vancouver BC V6T 1Z1, Canada
[30] University of Alberta, Department of Physics, Edmonton AB T6G 2J1, Canada
[31] Duke University, Dept of Physics, Durham, NC 27708-0305, USA
[32] Research Institute for Particle and Nuclear Physics, P O Box 49, H-1525 Budapest, Hungary
[33] Institute of Nuclear Research, P O Box 51, H-4001 Debrecen, Hungary
[34] Ludwigs-Maximilians-Universität München, Sektion Physik, Am Coulombwall 1, D-85748 Garching, Germany

Received: 25 June 1998 / Published online: 1 March 1999

**Abstract.** The Michel parameters of the leptonic $\tau$ decays are measured using the OPAL detector at LEP. The parameters $\rho_\ell$, $\xi_\ell$, $(\xi\delta)_\ell$ (with $\ell = \mathrm{e}, \mu$) and $\eta_\mu$ are extracted from the energy spectra of the charged decay leptons and from their energy–energy correlations. A new method involving a global likelihood fit of Monte Carlo generated events with complete detector simulation and background treatment has been applied to the data recorded at center-of-mass energies close to $\sqrt{s} = m_{\mathrm{Z}^0}$ corresponding to an integrated luminosity of 155 pb$^{-1}$. If e-$\mu$ universality is assumed and inferring the $\tau$ polarization from neutral current data, the measured Michel parameters are:

$$\begin{aligned} \rho &= 0.781 \pm 0.028 \pm 0.018, & \xi &= 0.98 \pm 0.22 \pm 0.10, \\ \eta &= 0.027 \pm 0.055 \pm 0.005, & \xi\delta &= 0.65 \pm 0.14 \pm 0.07, \end{aligned}$$

where the value of $\eta$ has been constrained using the published OPAL measurements of the leptonic branching ratios and the $\tau$ lifetime. Limits on non-standard coupling constants and on the masses of new gauge bosons are obtained. The results are in agreement with the V−A prediction of the Standard Model.

## 1 Introduction

A measurement of the Michel parameters in $\tau$ decays is presented which involves a novel method to fit the energy spectra and energy-energy correlations of the charged decay leptons. The $\tau$-pair data set used was produced in $e^+e^-$ collisions at center-of-mass energies close to $\sqrt{s} = m_{Z^0}$, corresponding to an integrated luminosity of 155 $pb^{-1}$. The parameters are fitted to the lepton spectra of three event classes, electron–hadron, muon–hadron and electron–muon, depending on the decay modes of the two $\tau$ decays in the event. Previous measurements of the Michel parameters in $\tau$ decays exist that were performed at LEP [1,2] and at other $e^+e^-$ colliders [3–11]. Unlike previous measurements the analysis presented makes use of a binned maximum likelihood fit of fully simulated events to the data. It accounts for radiative corrections, detector effects, background processes and selection efficiencies in a comparatively original way.

### 1.1 Lorentz structure

In the Standard Model the charged weak interaction is described by the exchange of left-handed W bosons, i.e.,

[a] and at TRIUMF, Vancouver, Canada V6T 2A3
[b] and Royal Society University Research Fellow
[c] and Institute of Nuclear Research, Debrecen, Hungary
[d] and Department of Experimental Physics, Lajos Kossuth University, Debrecen, Hungary
[e] on leave of absence from the University of Freiburg

by a pure vector coupling to only left-handed fermions. Thus, in the low-energy four-fermion ansatz, the Lorentz structure of the charged current is predicted to be of the type "V−A ⊗ V−A". With this formalism the dominant features of nuclear $\beta$ decay and of $\mu$ decay are correctly described [12]. Deviations from this behavior would indicate new physics and might be caused by changes in the W boson couplings or through interactions mediated by new gauge bosons [13]. The dominant contribution would then be either the one with the largest coupling or the one being mediated by the lightest boson. This means that if there exist contributions to the leptonic decay structure other than V−A, for example a right-handed vector coupling arising from a heavy right-handed W boson, $\mathrm{W_R}$, or a scalar coupling to a charged Higgs boson, these would emerge first in the decay of the massive $\tau$ lepton. Among all its decay modes, the decays $\tau \to \mathrm{e}\,\nu_\mathrm{e}\nu_\tau$ and $\tau \to \mu\,\nu_\mu\nu_\tau$ are the only ones in which the electroweak couplings can be probed without disturbance from the strong interaction. This makes the purely leptonic $\tau$ decays an ideal system for the study of the Lorentz structure of the charged weak current.

The leptonic decay amplitude can be generalized by adding current–current terms for all possible bilinear covariants. The most general, derivative-free, four-lepton interaction matrix element for the $\tau \to \ell\,\nu_\ell\nu_\tau$ decay that is local and Lorentz invariant can be written as (see e.g. [14]):

$$\mathcal{M} = 4\frac{G_0}{\sqrt{2}} \sum_{\substack{\gamma=\mathrm{S,V,T}\\ \epsilon,\omega=\mathrm{R,L}}} g^\gamma_{\epsilon\omega}\, \langle\, \overline{\ell}_\epsilon | \Gamma^\gamma | \nu_\ell \rangle\, \langle \overline{\nu}_\tau | \Gamma_\gamma | \tau_\omega \rangle. \qquad (1)$$

Here $\gamma$ denotes the type of the interaction (scalar, vector or tensor) and $\Gamma^\gamma$ are $4 \times 4$ matrices defined in terms of the Dirac matrices:

$$\begin{aligned} &\Gamma^\mathrm{S} = 1, \qquad \Gamma^\mathrm{V} = \gamma^\mu, \\ &\Gamma^\mathrm{T} = \frac{1}{\sqrt{2}}\,\sigma^{\mu\nu} \equiv \frac{i}{2\sqrt{2}}(\gamma^\mu\gamma^\nu - \gamma^\nu\gamma^\mu). \end{aligned} \qquad (2)$$

The indices $\omega$ and $\epsilon$ denote the chiralities of the $\tau$ lepton and its charged decay lepton, $\ell$, respectively. For given ($\omega$, $\epsilon$) the chiralities of the neutrinos are uniquely determined. Tensor interactions exist only for opposite chiralities of the charged leptons. This leads to 10 complex coupling constants, $g^\gamma_{\epsilon\omega}$, for which the Standard Model predicts $g^\mathrm{V}_\mathrm{LL}$=1 and all others being zero. Choosing the arbitrary phase by defining $g^\mathrm{V}_\mathrm{LL}$ to be real and positive leaves 19 real numbers to be determined by experiment. As long as one is interested in the relative strengths of the couplings, it is convenient to require the following normalization condition:

$$\begin{aligned} N \equiv \quad & \tfrac{1}{4}\left(|g^\mathrm{S}_\mathrm{LL}|^2 + |g^\mathrm{S}_\mathrm{LR}|^2 + |g^\mathrm{S}_\mathrm{RL}|^2 + |g^\mathrm{S}_\mathrm{RR}|^2\right) \\ & + \left(|g^\mathrm{V}_\mathrm{LL}|^2 + |g^\mathrm{V}_\mathrm{LR}|^2 + |g^\mathrm{V}_\mathrm{RL}|^2 + |g^\mathrm{V}_\mathrm{RR}|^2\right) \\ & + 3\left(|g^\mathrm{T}_\mathrm{LR}|^2 + |g^\mathrm{T}_\mathrm{RL}|^2\right) = 1. \end{aligned} \qquad (3)$$

This restricts the allowed ranges of the coupling constants to $|g^\mathrm{S}| \le 2$, $|g^\mathrm{V}| \le 1$ and $|g^\mathrm{T}| \le 1/\sqrt{3}$. The overall normalization can be incorporated into $G_0$ which then accounts for deviations from the Fermi constant $G_\mathrm{F}$.

### 1.2 Michel parameters

At the Born level, neglecting radiative corrections and terms proportional to $(m_\ell/m_\tau)^2$, only four different combinations of these coupling constants, denoted by $\rho$, $\xi$, $\delta$ and $\eta$, determine the shape of the decay spectra. In the $\tau$ rest frame, the leptonic decay width can, for massless neutrinos, be written as

$$\begin{aligned} \frac{\mathrm{d}^2\Gamma_{\tau\to\ell\,\nu_\ell\nu_\tau}}{\mathrm{d}\Omega\,\mathrm{d}x^*} = \frac{G_0^2 m_\tau^5}{192\pi^4}\, x^{*2} \Bigg\{ & 3(1-x^*) + \rho_\ell \left(\frac{8}{3}x^* - 2\right) \\ & + 6\,\eta_\ell \frac{m_\ell}{m_\tau}\frac{(1-x^*)}{x^*} \\ & - P_\tau\,\xi_\ell \cos\theta^* \left[(1-x^*) + \delta_\ell\left(\frac{8}{3}x^* - 2\right)\right]\Bigg\}. \end{aligned} \qquad (4)$$

Here $x^* = E^*_\ell/E^\mathrm{max}_\ell$ is the scaled energy of the charged decay lepton in the $\tau$ rest frame with $E^\mathrm{max}_\ell = (m_\tau^2 + m_\ell^2)/2m_\tau$ being its maximal energy and $\cos\theta^*$ is the angle between the $\tau$-spin direction and the momentum of the decay lepton. $P_\tau$ is the average $\tau$ polarization. After integration over $\cos\theta^*$ and boosting into the $\mathrm{Z}^0$ rest frame, the spectrum has the form:

$$H(x) = f(x) + P_\tau\, g(x), \qquad (5)$$

with

$$\begin{aligned} f(x) &= a(x) + \rho\, b(x) + \eta\, e(x), \\ g(x) &= \xi\, c(x) + \xi\delta\, d(x), \end{aligned} \qquad (6)$$

where $f(x)$ and $g(x)$ describe the isotropic and the $\tau$-spin-dependent part, respectively, and $a(x) \ldots e(x)$ are known third-order polynomials in the scaled energy $x = E_\ell/E_\tau$. Hence, allowing the most general couplings, the shape of the spectra can be described by the four Michel parameters [15,16] for which the Standard Model predicts the values $\rho = 3/4$, $\xi = 1$, $\delta = 3/4$ and $\eta = 0$ according to a V−A structure of the charged weak current. Their definitions read in detail:[1]

$$\begin{aligned} \rho = {} & \frac{3}{4}|g^\mathrm{V}_\mathrm{LL}|^2 + \frac{3}{4}|g^\mathrm{V}_\mathrm{RR}|^2 + \frac{3}{16}|g^\mathrm{S}_\mathrm{LL}|^2 + \frac{3}{16}|g^\mathrm{S}_\mathrm{LR}|^2 \\ & + \frac{3}{16}|g^\mathrm{S}_\mathrm{RL}|^2 + \frac{3}{16}|g^\mathrm{S}_\mathrm{RR}|^2 + \frac{3}{4}|g^\mathrm{T}_\mathrm{LR}|^2 + \frac{3}{4}|g^\mathrm{T}_\mathrm{RL}|^2 \\ & - \frac{3}{4}\mathrm{Re}(g^\mathrm{S}_\mathrm{LR} g^{\mathrm{T}*}_\mathrm{LR}) - \frac{3}{4}\mathrm{Re}(g^\mathrm{S}_\mathrm{RL} g^{\mathrm{T}*}_\mathrm{RL}), \\ \xi = {} & |g^\mathrm{V}_\mathrm{LL}|^2 + 3|g^\mathrm{V}_\mathrm{LR}|^2 - 3|g^\mathrm{V}_\mathrm{RL}|^2 - |g^\mathrm{V}_\mathrm{RR}|^2 + 5|g^\mathrm{T}_\mathrm{LR}|^2 \\ & - 5|g^\mathrm{T}_\mathrm{RL}|^2 + \frac{1}{4}|g^\mathrm{S}_\mathrm{LL}|^2 - \frac{1}{4}|g^\mathrm{S}_\mathrm{LR}|^2 + \frac{1}{4}|g^\mathrm{S}_\mathrm{RL}|^2 - \frac{1}{4}|g^\mathrm{S}_\mathrm{RR}|^2 \\ & + 4\mathrm{Re}(g^\mathrm{S}_\mathrm{LR} g^{\mathrm{T}*}_\mathrm{LR}) - 4\mathrm{Re}(g^\mathrm{S}_\mathrm{RL} g^{\mathrm{T}*}_\mathrm{RL}), \end{aligned} \qquad (7)$$

[1] Since by definition $\delta$ contains a factor $1/\xi$ it is convenient to use $(\xi\delta)$ instead of $\delta$.

$$\xi\delta = \frac{3}{4}|g^{\mathrm{V}}_{\mathrm{LL}}|^2 - \frac{3}{4}|g^{\mathrm{V}}_{\mathrm{RR}}|^2 + \frac{3}{16}|g^{\mathrm{S}}_{\mathrm{LL}}|^2 - \frac{3}{16}|g^{\mathrm{S}}_{\mathrm{LR}}|^2 + \frac{3}{16}|g^{\mathrm{S}}_{\mathrm{RL}}|^2 - \frac{3}{16}|g^{\mathrm{S}}_{\mathrm{RR}}|^2 - \frac{3}{4}|g^{\mathrm{T}}_{\mathrm{LR}}|^2 + \frac{3}{4}|g^{\mathrm{T}}_{\mathrm{RL}}|^2 + \frac{3}{4}\mathrm{Re}(g^{\mathrm{S}}_{\mathrm{LR}} g^{\mathrm{T}*}_{\mathrm{LR}}) - \frac{3}{4}\mathrm{Re}(g^{\mathrm{S}}_{\mathrm{RL}} g^{\mathrm{T}*}_{\mathrm{RL}})\,,$$

$$\eta = \frac{1}{2}\mathrm{Re}\left[ g^{\mathrm{V}}_{\mathrm{LL}} g^{\mathrm{S}*}_{\mathrm{RR}} + g^{\mathrm{V}}_{\mathrm{RR}} g^{\mathrm{S}*}_{\mathrm{LL}} + g^{\mathrm{V}}_{\mathrm{RL}}(g^{\mathrm{S}*}_{\mathrm{LR}} + 6 g^{\mathrm{T}*}_{\mathrm{LR}}) + g^{\mathrm{V}}_{\mathrm{LR}}(g^{\mathrm{S}*}_{\mathrm{RL}} + 6 g^{\mathrm{T}*}_{\mathrm{RL}}) \right].$$

One of the parameters, $\eta$, can also lead to a change in the leptonic decay width of the $\tau$ lepton.

If contributions from other couplings exist, they are not necessarily the same for $\tau \to \mathrm{e}\,\nu_{\mathrm{e}}\nu_\tau$ and $\tau \to \mu\,\nu_\mu\nu_\tau$. Therefore, the Michel parameters for decays into electron and muon are measured independently. Because the $\eta_\ell$ term is suppressed by a factor $m_\ell/m_\tau$, there is almost no sensitivity to $\eta_{\mathrm{e}}$ from the $\tau \to \mathrm{e}\,\nu_{\mathrm{e}}\nu_\tau$ decay spectrum. Thus in the following $\eta_{\mathrm{e}}$ is set to zero. This leaves the 7 parameters $\rho_{\mathrm{e}}$, $\xi_{\mathrm{e}}$, $(\xi\delta)_{\mathrm{e}}$, and $\rho_\mu$, $\xi_\mu$, $(\xi\delta)_\mu$, $\eta_\mu$ to be determined.

To test the Standard Model prediction the parameters will also be fitted under the assumption of e-$\mu$ universality. It is possible to test explicit extensions, for example by focusing on vector couplings, or by allowing only one additional scalar contribution. In this way, mass limits for a right-handed W boson, $\mathrm{W_R}$, as well as for a charged Higgs boson are determined.

### 1.3 Lepton–lepton correlations

At LEP, $\tau$ pairs are produced with almost perfect spin correlation.[2] This allows one to measure the spin-dependent part of the decay spectra with high sensitivity by employing the correlations between both $\tau$ decays in the event [17,18]. For parallel $\tau$ spins the correlation function can be written as

$$I(x_1, x_2) = f(x_1)f(x_2) + g(x_1)g(x_2) - P_\tau\left[\, f(x_1)g(x_2) + f(x_2)g(x_1)\,\right], \qquad (8)$$

where $f(x)$ and $g(x)$ are the above third-order polynomials and $P_\tau$ is the average polarization of the $\tau^-$ lepton. In contrast to uncorrelated single decay spectra (5) here the product of the two spin-dependent parts, $g(x_1)g(x_2)$, without the suppression by the $\tau$ polarization. Thus, in the case of two leptonic decays in the event, the correlation function provides high sensitivity to the parameters $\xi$ and $\xi\delta$, whereas the more frequent events with single leptonic decays contribute with high statistics to the measurement of $\rho$ and $\eta$.

[2] For V- and A-type couplings in the production, the $\tau^+$ and $\tau^-$ have opposite chiralities.

### 1.4 Tau polarization

In addition to the charged current couplings which determine the decay of the $\tau$ lepton, the couplings to the neutral current which are responsible for the $\tau$ production influence the shape of the spectra. The difference in the left- and right-handed $\mathrm{Z}^0$ couplings causes the $\tau$ leptons to be produced polarized affecting the spin-dependent part of the decay spectra. In principle, the average $\tau$ polarization, $P_\tau$, could be measured along with the Michel parameters. However, this introduces additional correlations between the fit parameters and limits the accuracy of the Michel parameter measurements while it does not reveal anything new about the decay structure. Since extensions to the charged sector of the weak interaction do not a priori change the neutral current, a different approach is pursued in this analysis. Instead of testing both sectors simultaneously at the expense of sensitivity, the charged current is investigated in the most general way, while the neutral current (i.e., the $\tau$ polarization) is assumed to be described by the Standard Model couplings with adequate accuracy.

Since all direct measurements of $P_\tau$ from $\mathrm{e^+e^-} \to \tau^+\tau^-$ data at $\sqrt{s} = m_{\mathrm{Z}^0}$ implicitly have assumed a V−A coupling in the $\tau$ decay, the use of these results as input to this analysis would introduce a bias. Therefore, measurements of the neutral current which are independent of the charged sector have been used to calculate $P_\tau$ using the ZFITTER[19] package. The uncertainty arising from this procedure has been studied with the systematic errors. Its impact on the Michel parameter measurement is smaller than the one that would have been introduced through correlations between the parameters and the polarization if $P_\tau$ was fitted.

As input to the $P_\tau$ calculation the following values were used [20]: the preliminary LEP measurement of the $\mathrm{Z}^0$ mass $m_{\mathrm{Z}^0} = (91.1884 \pm 0.0022)\,\mathrm{GeV}$, the CDF/DØ combined value for the top mass $m_{\mathrm{t}} = (175 \pm 6)\,\mathrm{GeV}$, $m_{\mathrm{H}^0} = 300\,\mathrm{GeV}$ with $60\,\mathrm{GeV} < m_{\mathrm{H}^0} < 1\,\mathrm{TeV}$, $\alpha_{\mathrm{s}}(m_{\mathrm{Z}^0}) = 0.118 \pm 0.003$ and $\alpha(m_{\mathrm{Z}^0})^{-1} = 128.90 \pm 0.09$. These values yield the predicted value of the $\tau$ polarization at the $\mathrm{Z}^0$ peak as $P_\tau = -0.1391^{\,+0.0069}_{\,-0.0055}$, where the dominant uncertainty is due to the unknown Higgs boson mass. In this analysis, data taken at $\sqrt{s} = m_{\mathrm{Z}^0}$ are used together with data below and above $m_{\mathrm{Z}^0}$. Averaging over the energy dependence of $P_\tau$ according to the data set used yields the same quoted value. Over the full range this leads to an uncertainty in $P_\tau$ of approximately 5%, which is still smaller than the error of the current measurements (see e.g. [21]).

## 2 Event selection

### 2.1 OPAL detector

The OPAL detector is described in detail elsewhere [22, 23]. Here, only a brief summary of the main components shall be given. The innermost subdetector is a microvertex detector with two layers of double-sided silicon strips. It is enclosed by a system of three different drift

chambers, a precision vertex chamber with axial and stereo wire readout, a large cylindrical drift volume (jet chamber) with 24 azimuthal sectors of 159 signal wires each, and a surrounding set of $z$ chambers with wires perpendicular to the beam direction. The central tracking system is contained inside a magnetic coil which provides a solenoidal field of 0.435 Tesla. This leads to a resolution of the transverse momentum of $\sigma_{p_t}/p_t \approx 1.5 \times 10^{-3}\, p_t\,(\mathrm{GeV})$. In addition, the specific energy loss, $\mathrm{d}E/\mathrm{d}x$, of charged particles is measured in the jet chamber. The electromagnetic calorimeter (ECAL) is built of 11 704 lead glass blocks of approximately $25\,X_0$ radiation lengths, providing an energy resolution of typically $\sigma_E/E \approx 12\%/\sqrt{E\,(\mathrm{GeV})}$. In front of the ECAL, a thin gas detector (the presampler) measures electromagnetic showers beginning in the material of the inner detector components. The ECAL is surrounded by the iron return yoke of the magnet which is instrumented with limited streamer tubes to serve as a hadron calorimeter (HCAL). The whole detector is enclosed by four layers of muon chambers, giving the position and the direction of the penetrating particles.

As observables for the fit, different variables in the two leptonic decay channels are chosen. In case of the $\tau \to \mu\,\nu_\mu\nu_\tau$ decays, the track momentum of the muon measured in the jet chamber, $p_{\mathrm{track}}$, is taken, whereas for the $\tau \to \mathrm{e}\,\nu_\mathrm{e}\nu_\tau$ decays the energy deposited by the electron in the electromagnetic calorimeter, $E_{\mathrm{cluster}}$, is used. The cluster energy includes a large fraction of final state photon radiation from the electron and is thus less dependent on the modeling of the photon radiation in the generator and the detector simulation. Both variables are scaled to the beam energy which is used as the estimator for the maximal energy of the decay lepton.

### 2.2 Tau pair selection

From the data collected with the OPAL detector during the years 1990–1995, $\tau$-pair events are selected in several steps. The selection follows the strategy described in earlier OPAL publications [21,24] and given in detail in [25]. First, lepton pairs are preselected by requiring exactly two charged jet-cones of 35° half-opening angle with low track and cluster multiplicity. Two-photon events are rejected by requiring either a large visible energy or an unbalanced transverse momentum sum, and a small acollinearity.

From this sample, Bhabha events are removed based on a large sum of cluster energies or a large sum of track momenta in conjunction with large cluster energies. Afterwards, $\mu$-pair events are eliminated if consistent with high track momenta, small energy deposit in the calorimeter or signals in the muon chambers. The remaining 147 042 events are almost entirely $\tau$ pairs (see Sect. 2.5 for the remaining background in the used event classes). The geometrical acceptance of this selection covers the region $|\cos\theta| < 0.95$.

### 2.3 Tau decay mode identification

A likelihood selection is used to identify the $\tau$ decay modes in the two cones. It distinguishes between the 1-prong decays $\tau \to \mathrm{e}\,\nu_\mathrm{e}\nu_\tau$, $\tau \to \mu\,\nu_\mu\nu_\tau$ and $\tau \to \mathrm{h}\,\nu_\tau$ where h is either $\pi$/K, $\rho$ or $\mathrm{a}_1 \to \pi 2\pi^0$. It makes use of a set of variables which allow the discrimination of different channels.[3] These variables include:

- $E_{\mathrm{cluster}}/p_{\mathrm{track}}$ – the ratio of the energy deposited in the electromagnetic calorimeter (ECAL) with respect to the track momentum measured in the central detector,
- $\mathrm{d}E/\mathrm{d}x$ – the specific energy loss in the jet chamber,
- $N^{90\%}_{\mathrm{blocks}}$ – the number of ECAL blocks that contain 90% of the measured energy in the cluster associated to the track,
- $E_{\mathrm{neutral}}/E_{\mathrm{cone}}$ – the fraction of ECAL energy in the cone that is not associated to the track,
- $(\Delta\phi)_{\mathrm{max}}$ – the maximum angle between the track and a presampler cluster assigned to the cone,
- $W_{\mathrm{pres}}$ – the width of the largest presampler cluster,
- $N_{\mathrm{hits}}/N_{\mathrm{layers}}$ – the average number of hits per active layer in the hadronic calorimeter (HCAL),
- $N_{7\mathrm{hits}}$ – the number of hits in the last three HCAL layers and in the four layers of the muon chambers,
- $W_{\mathrm{muon}}$ – the matching probability between the extrapolated track and a muon chamber track segment.

The measured variables are then compared to a set of reference distributions that have been produced by a Monte Carlo simulation of the considered decay modes (see Sect. 3.3).

Based on the variable $x_i$, the expected fraction of decay modes of the type $j$ is given as

$$\ell_i^j(x_i) = \frac{f_i^j(x_i)}{\sum_{j=1}^{N_{\mathrm{modes}}} f_i^j(x_i)}\,, \tag{9}$$

where $f_i^j$ are the normalized probability densities taken from the reference distribution for the respective variable $i$ and $N_{\mathrm{modes}} = 5$ is the number of considered decay modes. The information from all the variables is then combined into the product likelihood for the hypothesis $j$:

$$\mathcal{L}^j(x_1,\ldots,x_{N_{\mathrm{variables}}}) = \prod_{i=1}^{N_{\mathrm{variables}}} \ell_i^j(x_i)\,. \tag{10}$$

Normalized to all considered alternatives the expression yields the relative likelihood of the decay being of type $j$:

$$P^j = \frac{\mathcal{L}^j}{\sum_{j=1}^{N_{\mathrm{modes}}} \mathcal{L}^j}\,, \tag{11}$$

[3] Kaons are not separated from pions and are counted among the corresponding $\pi$ channels in the following.

**Table 1.** Efficiencies in % for the likelihood identification of 1-prong $\tau$ decay modes within the fiducial region. The diagonal values are the efficiencies for the true identified modes whereas the off-diagonal values represent the misidentification probabilities

| | Identified mode | | | | |
|---|---|---|---|---|---|
| Generated mode | $\tau \to \mathrm{e}\,\nu_\mathrm{e}\nu_\tau$ | $\tau \to \mu\,\nu_\mu\nu_\tau$ | $\tau \to \pi\,\nu_\tau$ | $\tau \to \rho\,\nu_\tau$ | $\tau \to \mathrm{a}_1\,\nu_\tau$ |
| $\tau \to \mathrm{e}\,\nu_\mathrm{e}\nu_\tau$ | 96.5 | – | 1.1 | 1.7 | 0.7 |
| $\tau \to \mu\,\nu_\mu\nu_\tau$ | 0.3 | 92.2 | 7.0 | 0.5 | – |
| $\tau \to \pi\,\nu_\tau$ | 1.4 | 3.3 | 82.1 | 9.5 | 3.6 |
| $\tau \to \rho\,\nu_\tau$ | 0.3 | 0.2 | 10.3 | 67.8 | 21.3 |
| $\tau \to \mathrm{a}_1\,\nu_\tau$ | 0.1 | – | 1.3 | 25.8 | 72.7 |

which in the case of uncorrelated variables can be interpreted as a probability. To obtain high-purity samples, the cones involving the lepton are required to be identified with a relative likelihood of $P^j > 90\%$. The simulated reference distributions are checked against the data by using a tagging technique. For that purpose, the likelihood variables of each detector component are compared between data and Monte Carlo based on a clear decay mode identification from the other components. A comparison of some of the variables can be found in [26].

## 2.4 Selection efficiency

Throughout the analysis, the simulated events and the data are treated in an identical manner. Thus, the efficiencies for the event selection and the decay mode identification are accounted for in the fit as modeled in the Monte Carlo samples. The validity of the simulation has been tested by comparing Monte Carlo efficiencies as a function of energy/momentum with data control samples (see Sect. 4.1). Table 1 lists the efficiencies for the decay mode identification within the fiducial volume of $|\cos\theta| < 0.95$. The inefficiency of the muon channel originates mainly from the low-$x$ region where the separation from pions becomes poorer.

Based on the decays of both $\tau$ leptons, the events are divided into mutually exclusive samples: lepton–lepton correlations (e–$\mu$) and single-lepton decays (e–hadrons, $\mu$–hadrons). As mentioned in Sect. 1.3, the correlation spectra have a high sensitivity to the spin-dependent parameters ($\xi$, $\xi\delta$) while the single decays provide high statistics for the isotropic parameters ($\rho$, $\eta$).

Decay correlations in e–e and $\mu$–$\mu$ events are subject to a large background contamination from $\mathrm{e^+e^-} \to \mathrm{e^+e^-}$ and $\mathrm{e^+e^-} \to \mu^+\mu^-$ processes as well as from two-photon events $\gamma\gamma \to \mathrm{e^+e^-}$ and $\gamma\gamma \to \mu^+\mu^-$. These background sources distort the correlation spectra in the two most sensitive regions where both leptons have high energies or both have low energies, respectively. Due to the uncertainties in the estimation of these backgrounds, the e–e and $\mu$–$\mu$ event classes would contribute with a dominant systematic error to the fit result. For this reason they are not included in this analysis.

In Table 2 the overall efficiencies for the three event classes are given. The additional inefficiencies with respect to the decay mode identification arise from geometrical cuts that are performed on the individual event classes to exclude insensitive or inadequately simulated regions of the detector. These regions include the proximity of the anode wire planes of the jet chamber, $\phi_\mathrm{sector} < 0.4°$, the extreme forward region of the electromagnetic calorimeter, $|\cos\theta| > 0.9$, and a few small regions not covered by the muon chambers.

**Table 2.** Selection efficiencies for the three event considered classes

| | Event Class | | |
|---|---|---|---|
| | $\tau_1 \to \mathrm{e}\,\nu_\mathrm{e}\nu_\tau$ $\tau_2 \to \mathrm{h}\,\nu_\tau$ | $\tau_1 \to \mu\,\nu_\mu\nu_\tau$ $\tau_2 \to \mathrm{h}\,\nu_\tau$ | $\tau_1 \to \mathrm{e}\,\nu_\mathrm{e}\nu_\tau$ $\tau_2 \to \mu\,\nu_\mu\nu_\tau$ |
| Sample size | 19369 | 21190 | 5834 |
| Efficiency | 83.1% | 88.6% | 85.8% |

Figures 1a,b show the selection efficiencies for the single leptonic decay samples e–h and $\mu$–h as a function of the scaled energy $x_E$ and scaled momentum $x_p$, respectively.

## 2.5 Background

Various sources of background in the $\tau$-pair sample and in the $\tau \to \mathrm{e}\,\nu_\mathrm{e}\nu_\tau$ and $\tau \to \mu\,\nu_\mu\nu_\tau$ samples have been investigated. The main contribution comes from misidentification of the hadronic $\tau$ decays. Due to the distinctive signatures of electrons and muons in the detector, cross-talk between the two channels is negligible. The main backgrounds for the $\tau \to \mathrm{e}\,\nu_\mathrm{e}\nu_\tau$ mode originate from $\tau \to \pi\,\nu_\tau$ and $\tau \to \rho\,\nu_\tau$ decays. For the $\tau \to \mu\,\nu_\mu\nu_\tau$ mode the dominant background source are $\tau \to \pi\,\nu_\tau$ decays. Table 3 lists the different backgrounds in the three event samples. For simplicity, the three identified hadron channels have been summed up. For the single decay spectra, double lepton events in which the recoil lepton has been misidentified as a hadron are also quoted as background.

Furthermore, Bhabha and $\mu$-pair events may pass the selection and contaminate the samples. This can occur, for example, for an $\mathrm{e^+e^-} \to \mathrm{e^+e^-}$ event where one electron is misidentified as a $\tau \to \rho\,\nu_\tau$ decay, or to an $\mathrm{e^+e^-} \to \mu^+\mu^-$ event where one muon fakes a $\tau \to \pi\,\nu_\tau$ decay.

As mentioned earlier, the presented method allows us to account for all backgrounds that are simulated in the Monte Carlo. Since either the background shapes do not

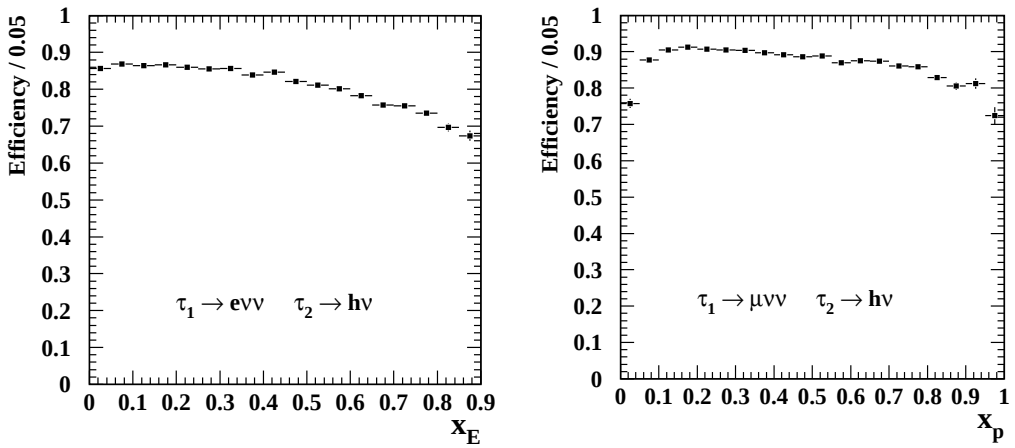


**Fig. 1.** Selection efficiencies for the e–h ($\mu$–h) event samples as a function of the scaled lepton energy (momentum), $x_E$ ($x_p$), as determined from the Monte Carlo after the preselection including all fiducial cuts

**Table 3.** Identified events and background from $\tau$ decays, Bhabha, $\mu$-pair and two-photon events. For simplicity the three hadronic channels have been summed up

| Background source | | Event class | | |
|---|---|---|---|---|
| | | e–h | $\mu$–h | e–$\mu$ |
| leptonic $\tau$ | e–e | 0.73% | – | 0.00% |
| | e–$\mu$ | 1.70% | – | |
| | $\mu$–e | – | 0.99% | |
| | $\mu$–$\mu$ | – | 1.64% | 0.12% |
| hadronic $\tau$ | h–h | 0.72% | 1.55% | – |
| | e–h | | – | 1.73% |
| | h–$\mu$ | – | | 0.78% |
| non-$\tau$ | e e $\to$ e e | 0.06% | – | 0.00% |
| | e e $\to \mu\mu$ | – | 0.56% | 0.06% |
| | $\gamma\gamma \to$ e e | 0.03% | – | 0.00% |
| | $\gamma\gamma \to \mu\mu$ | – | 0.21% | 0.04% |
| Total | | 3.3% | 5.0% | 2.8% |

depend on the Michel parameters (hadronic and non-$\tau$ background) or their dependence has, due to the small fraction, no significant impact on the shape of the signal distribution, the residual events can be independently added to the fit spectrum.

## 3 Fitting method

To extract the Michel parameters from the observed spectra, a binned maximum likelihood fit of a set of Monte Carlo spectra has been applied to the data. Compared to fits that involve analytical functions to describe the data distributions, this method has several advantages. It includes radiative corrections at the generator level where their description is more easily accessible than it is through the convolution of photon radiation probability functions. It provides a full simulation of the detector response and thus accounts for the energy and momentum resolution as well as for the selection efficiency in an elegant way. It also accounts for contamination from misidentified $\tau$ decays and from other background sources, like Bhabha events, $\mu$-pair events and two-photon events. This makes it unnecessary to unfold resolution and efficiency effects from the data. A particular benefit is that selection criteria which restrict the phase space do not present a problem for the fit because all requirements can be placed identically on data and Monte Carlo. In addition, observables for each decay mode can be chosen to accommodate the particular capabilities of the detector rather than to facilitate the theoretical description.

### 3.1 Linear combination

Since the single decay spectra depend linearly on the Michel parameters, it is possible to decompose any observed spectrum into different basis spectra with each representing a specific set of parameters. To describe the whole parameter space including the constant term, five spectra have to be mixed with coefficients that add up to unity. For a particular choice of the basis parameter sets, the corresponding coefficients can be calculated by solving the respective equation system. This allows one to determine the values of the four Michel parameters by fitting the coefficients with respect to a given basis (i.e. the relative contributions of the basis spectra) to the data.

In the case of the energy-energy correlation spectra between two leptonic decays in each event (double decay spectra) this method is still applicable. These spectra can be represented by a composition that is bilinear in the $2\times4$ Michel parameters of the $\tau$ decays into electron and muon (or of second order in the four parameters if the leptons in both hemispheres are identical). The correlation basis is then the tensor product of two single decay bases. Now, 25 coefficients appear in the decomposition, which are not all independent. From these, the $2 \times 4$ Michel parameters for e and $\mu$ decays, respectively, can again be calculated by matrix inversion (see Sect. 3.2). In this formalism, the e–e and $\mu$–$\mu$ correlations with only 4 free Michel parameters

are just a special case of the e-$\mu$ correlations.[4] They will not be discussed explicitly since they are not used for the analysis.

With this method, which is based on Monte Carlo event generation, it is possible to describe any value of the Michel parameters with a finite sample of events by varying the appropriate contribution to the spectrum.

### 3.2 Parameter basis

To describe the entire Michel parameter space, a basis has to be chosen which accounts for any possible combination. It is obvious that the parameter sets corresponding to pure S, P, V, A, T couplings do not fulfill this requirement because they do not involve any interference terms between different couplings. Also, the canonical basis with $(\rho, \xi, \xi\delta, \eta) = (1,0,0,0), (0,1,0,0), \ldots$ etc. is not physically meaningful, because it is not possible to have $\xi\delta$=1 and all other Michel parameters zero. However, it is desirable to have a "nearly orthogonal" set in order to avoid large correlations between the coefficients. Examples of different couplings and the corresponding Michel parameters can be found in Table 10.

Taking this into consideration, the following basis has been chosen:

$$\begin{pmatrix} \rho \\ \xi \\ \xi\delta \\ \eta \end{pmatrix} = c_1 \begin{pmatrix} 3/4 \\ 1 \\ 3/4 \\ 0 \end{pmatrix} + c_2 \begin{pmatrix} 1 \\ 0 \\ 0 \\ 0 \end{pmatrix} + c_3 \begin{pmatrix} 0 \\ 1 \\ 0 \\ 0 \end{pmatrix} + c_4 \begin{pmatrix} 3/4 \\ 0 \\ 0 \\ 1/2 \end{pmatrix} + c_5 \begin{pmatrix} 0 \\ 0 \\ 0 \\ 0 \end{pmatrix}, \quad (12)$$

with $\sum_i c_i = 1$. Here, each vector on the right-hand side stands for a spectrum generated with the quoted set of Michel parameters.

In a more general notation,[5] one can write for the case of the single lepton spectra

$$\mathbf{q}_\ell = M_\ell \cdot \mathbf{c}_\ell, \quad (13)$$

where $\mathbf{q}_\ell$ is the vector $(1, \rho_\ell, \xi_\ell, \delta_\ell, \eta_\ell)$, $\mathbf{c}_\ell$ is the vector of coefficients $(c_1, c_2, c_3, c_4, c_5)$, and $M_\ell$ is a $5\times5$ matrix given by

$$M_\ell = \begin{pmatrix} 1 & 1 & 1 & 1 & 1 \\ \rho_{\ell 1} & \rho_{\ell 2} & \rho_{\ell 3} & \rho_{\ell 4} & \rho_{\ell 5} \\ \xi_{\ell 1} & \xi_{\ell 2} & \xi_{\ell 3} & \xi_{\ell 4} & \xi_{\ell 5} \\ \delta_{\ell 1} & \delta_{\ell 2} & \delta_{\ell 3} & \delta_{\ell 4} & \delta_{\ell 5} \\ \eta_{\ell 1} & \eta_{\ell 2} & \eta_{\ell 3} & \eta_{\ell 4} & \eta_{\ell 5} \end{pmatrix}. \quad (14)$$

Here $\rho_{\ell_1}$ denotes the value of $\rho_\ell$ in the first basis spectrum, $\rho_{\ell_2}$ its value in the second spectrum and so forth. Hence, for a given set of Michel parameters the coefficients with respect to the basis $M_\ell$ can be calculated from

$$\mathbf{c}_\ell = (M_\ell)^{-1} \cdot \mathbf{q}_\ell. \quad (15)$$

Analogously, for the case of the double e-$\mu$ spectra one can write

$$\mathbf{q}_{e\mu} = M_{e\mu} \cdot \mathbf{c}_{e\mu}, \quad (16)$$

where the vector $\mathbf{q}_{e\mu}$ is the outer product of the vectors $\mathbf{q}_e$ and $\mathbf{q}_\mu$ ( $q_{e\mu_{ij}} = q_{ei} \cdot q_{\mu_j}$ ), $M_{e\mu}$ is the corresponding outer product of the matrices $M_e$ and $M_\mu$, and $\mathbf{c}_{e\mu} = (c_1, \ldots, c_{25})$ is the coefficient vector. Again, for a given set of 8 Michel parameters the corresponding 25 coefficients in the actual basis are obtained by multiplying the vector $\mathbf{q}_{e\mu} = (1, \rho_e, \xi_e, \delta_e, \eta_e, \rho_\mu, \rho_e\rho_\mu, \xi_e\rho_\mu, \ldots, \eta_e\eta_\mu)$ with the inverse of the $25 \times 25$ matrix $M_{e\mu}$.

### 3.3 Monte Carlo simulated samples

The $\tau$-pair Monte Carlo sample was generated using the KORALZ-3.8 [27] generator and a modified version of the TAUOLA-1.5 [28] decay library which was extended to include the full generalized matrix element [29]. This allows the variation of the Michel parameters over their whole range.

The TAUOLA-1.5 version was preferred over the newer version TAUOLA-2.4 [30,31] since it has a more general approach to real photonic corrections. The TAUOLA-1.5 library uses a factorization ansatz in order to produce real photons, where each charged particle radiates independently of its decay matrix element by internally applying the PHOTOS[32] package. On the other hand, the newer version TAUOLA-2.4 contains full $\mathcal{O}(\alpha)$ corrections to take the interference between photons radiated from the $\tau$ and photons radiated from the decay lepton into account. Although this might be more precise in the low-energy regime, it assumes a V−A type of interaction and is thus model dependent. The former version, TAUOLA-1.5, is capable of producing photons for all possible decay structures at a reasonable level of accuracy. It has therefore been chosen for this analysis.

Since finite Monte Carlo samples are used to describe possibly small variations in the shape of the spectra, it is vital to keep statistical fluctuations under control. If the distinct spectra were generated independently their differences would be smeared by Gaussian errors. In particular, it could happen that in a certain bin, the theoretical prediction for one spectrum is higher than for another but the generated number of events is lower. To avoid such fluctuations, each event is used for as many spectra as possible. This means that most of the Monte Carlo spectra share a large fraction of common events. An acceptance/rejection method is used where an event is flagged as accepted for each spectrum for which the generated random weight is below the prediction (and not just the standard V−A) and it is rejected only if it belongs to none of the considered spectra. This procedure guarantees that the difference of any two spectra has the right sign in all bins. As a side

[4] They are formally analog to e–$\mu$-correlations under the assumption of e–$\mu$ universality.

[5] To simplify the notation, $\delta$ is written instead of $\xi\delta$ in this section.

effect, it makes the generation of the Monte Carlo samples much more efficient.

Non-$\tau$ background sources such as Bhabha, $\mu$-pair and two-photon events have been generated by using the BABAMC[33,34], KORALZ[35] and VERMASEREN[36,37] generators, respectively. The response of the detector to generated particles is modeled using a simulation program [38] based on the GEANT[39] package. The simulated detector response has been checked with various control samples (see Sect. 4.1).

### 3.4 Fitting procedure

The appropriate Monte Carlo distributions, each representing a basis parameter set, are prepared with the identical binning as used for the observed lepton spectra. The coefficients of the spectra, $\mathbf{c}_\ell$, are determined using a binned maximum likelihood fit to the data. To avoid any dependence on the description of the overall efficiency, no constraint is made on the overall normalization. Since the coefficients are not independent, they are not varied themselves, but are calculated from the corresponding Michel parameters, as has been explained above. Thus, the Michel parameters are varied and fitted directly. The actual minimization and the determination of the covariance matrix is performed with the MINUIT[40] package. In doing this, a likelihood is computed for every mixture, assuming Poisson errors in each bin. Although the generated Monte Carlo sample is roughly four times larger than the data sample, some spectra still have bins with only few entries. This occurs in particular in the correlation distributions in regions of high $(x_1, x_2)$ as the various couplings may differ drastically for extreme momentum configurations. It is known that, in the case of small bin entries, ignoring the Monte Carlo errors biases the mean value of the fit and underestimates its spread. Therefore, fluctuations of both data and Monte Carlo have been taken into account. To accomplish this, an adjusted likelihood is calculated [41] by finding in each bin $i$ the most probable expectation with which data and Monte Carlo are consistent:

$$\ln \mathcal{L} = \sum_{i=1}^{N_{\text{bins}}} \sum_{j=1}^{N_{\text{spectra}}} (a_{ji} \ln A_{ji} - A_{ji}) + \sum_{i=1}^{N_{\text{bins}}} (d_i \ln f_i - f_i)\,. \tag{17}$$

Here $N_{\text{spectra}}$ is the number of Monte Carlo basis spectra (5 or 25), $d_i$ is the observed number of data events, $a_{ji}$ is the generated number of Monte Carlo events in spectrum $j$ and $A_{ji}$ is the best estimator for the Monte Carlo in the light of the data. The Monte Carlo expectation $f_i = \sum_j p_j A_{ji}$ is the composition of the best estimators using the mixing coefficients $p_j$. The first term of the adjusted likelihood (17) accounts for the agreement between the actual Monte Carlo distribution $(a_{ji})$ and the ideal distribution $(A_{ji})$ for all spectra $j$. The second term accounts for the agreement between the ideal composition $(f_i)$ and the data $(d_i)$. The likelihood is maximized with respect to both the coefficients $p_j$ and the estimators $A_{ji}$.[6] In the case of the double lepton spectrum, the index $i$ is replaced by two indices. For clarity, all the following expressions correspond to the single lepton spectra. The generalization to the double lepton case is straightforward.

The above equation represents the correct treatment of the problem, provided that the generated numbers, $a_{ji}$, are statistically independent. As described before, this is not the case for the prepared Monte Carlo spectra because they have (most) events in common. It is, however, possible to rewrite the expectation in each individual bin by means of independent numbers. To this end, the spectra are ordered by increasing numbers of events in the considered bin, and the coefficients are recalculated in terms of the differences between the bins as follows. If one writes for a particular composition (setting $b_{0i} := 0$):

$$f_i' = \sum_{j=1}^{N_{\text{spectra}}} c_j\, b_{ji} = \sum_{j=1}^{N_{\text{spectra}}} p_j\, (b_{ji} - b_{j-1,i}), \tag{18}$$

where $b_{ji}$ is the generated number of events in bin $i$ of basis spectrum $j$, then the differences $a_{ji} = b_{ji} - b_{j-1,i}$ are all independent. It follows that

$$p_j = \sum_{k=j}^{N_{\text{spectra}}} c_k, \tag{19}$$

where the coefficients $c_k$ are expressed in terms of the Michel parameters as described above (Sect. 3.2):

$$c_k = (M^{-1})_{kl} \cdot q_l. \tag{20}$$

After this transformation the above expression for the likelihood is applied.

### 3.5 Constraint on the $\eta$ parameter

It has been mentioned in Sect. 1.2 that the Michel parameter $\eta$ corresponds to a change in the partial decay width when it deviates from zero. However, to eliminate any dependence on the overall efficiency, Monte Carlo predictions are always normalized to the data. Due to the large correlation of $\eta$ with the $\rho$ parameter, configurations are possible where the spectral shape is changed only slightly while the value of $\eta$ is inconsistent with the observed branching ratio.[7]

Such a situation is avoided by constraining the branching ratios to their measured values throughout the fit. In the general ansatz for the Lorentz structure, the leptonic width is in lowest order changed to

$$\Gamma_\ell(\eta_\ell) = \Gamma_\ell^{(\text{SM})} \left(1 + 4\eta_\ell \frac{m_\ell}{m_\tau}\right), \tag{21}$$

[6] For each set of coefficients $p_j$ the numbers $A_{ji}$ can be calculated by solving an equation system.

[7] It has been shown that the leptonic branching ratios provide a sensitive observable on the Michel parameter $\eta$ [42].

where $\Gamma_\ell^{(\mathrm{SM})}$ is the Standard Model width (see e.g. [43]). From the measurement of the $\tau$ lifetime, $\tau_\tau$, the expected branching ratio, $B_\ell \equiv B(\tau \to \ell\,\nu_\ell\nu_\tau)$, depending on the value of $\eta_\ell$ can be calculated as

$$B_\ell(\eta_\ell) = \Gamma_\ell(\eta_\ell)\,\tau_\tau. \tag{22}$$

This relation can be used to calculate the most probable value of $\eta$,

$$\widehat{\eta_\ell} = \frac{1}{4}\frac{m_\tau}{m_\ell}\left(\frac{B_\ell}{\Gamma_\ell^{(\mathrm{SM})}\,\tau_\tau} - 1\right). \tag{23}$$

Using the published OPAL results for the $\tau \to \mu\,\nu_\mu\nu_\tau$ branching ratio, $B_\mu = 0.1736 \pm 0.0027$ [44], and the $\tau$ lifetime, $\tau_\tau = (289.2 \pm 2.1)$ fs [45], one determines

$$\widehat{\eta_\mu} = 0.032 \pm 0.073, \tag{24}$$

which is consistent with zero. The constraint to $\eta$ is applied by adding the following term to the log likelihood:

$$\ln \mathcal{L}_\ell^{\text{constraint}} = -\frac{1}{2}\,\frac{(\Gamma_\ell(\eta_\ell)\,\tau_\tau\ - B_\ell)^2}{(\Gamma_\ell(\eta_\ell)\,\Delta\tau_\tau\ )^2 + (\Delta B_\ell)^2}. \tag{25}$$

The use of this constraint makes the fit result for $\eta_\mu$ dominated by the branching ratio and lifetime measurements while the other parameters are still sensitive to the allowed variation in the $\eta_\mu$-dependent part of the shape. It has to be noted that the constrained value of $\eta_\mu$ assumes the total strength of the $\tau$–$\mu$ coupling to be universal.

### 3.6 Checks of the fitting method

To verify the reliability of the fit method, various checks have been performed with the Monte Carlo event samples. First, it has been tested that the fit of the linear composition can reproduce the genuine parameters of a specifically generated sample. It has also been proven that any genuine spectrum and its corresponding mixture of basis spectra are consistent within the statistical errors.

Second, the statistical errors of the fit parameters have been checked. For that purpose, the Monte Carlo sample has been divided into several pairs of subsamples with each pair representing a fit sample and a fake data sample. Then the fit has been performed for each subset separately, and the distribution of the fit result has been checked. It has been verified that, when the adjusted likelihood is applied, the individual errors are consistent with the spread of the mean values.

Third, it has been checked whether the particular choice of the parameter basis affects the fit results. Other sets of basis spectra than the quoted one have been used to describe a given Monte Carlo distribution. While some bases turned out to be less sensitive to one or more of the parameters, all alternatives have been found to be consistent within their fit errors.

**Table 4.** Results of the global fit to the e–h, $\mu$–h and e–$\mu$ energy spectra. The first error reflects both data and Monte Carlo statistics, the second error is systematic (see Sect. 4.1). The error on $\eta_\mu$ includes the errors on the muonic branching ratio and the $\tau$ lifetime

| $\tau \to \mathrm{e}\,\nu_\mathrm{e}\nu_\tau$ | | $\tau \to \mu\,\nu_\mu\nu_\tau$ | |
|---|---|---|---|
| $\rho_\mathrm{e}$ | $0.779 \pm 0.047 \pm 0.029$ | $\rho_\mu$ | $0.777 \pm 0.044 \pm 0.016$ |
| $\xi_\mathrm{e}$ | $1.13 \pm 0.39 \pm 0.14$ | $\xi_\mu$ | $0.79 \pm 0.41 \pm 0.09$ |
| $(\xi\delta)_\mathrm{e}$ | $0.72 \pm 0.31 \pm 0.14$ | $(\xi\delta)_\mu$ | $0.63 \pm 0.23 \pm 0.05$ |
| $\eta_\mathrm{e}$ | 0 (fixed) | $\eta_\mu$ | $0.010 \pm 0.065 \pm 0.001$ |

**Table 5.** Correlation coefficients between the parameters of the global fit

| | $\xi_\mathrm{e}$ | $(\xi\delta)_\mathrm{e}$ | $\rho_\mu$ | $\xi_\mu$ | $(\xi\delta)_\mu$ | $\eta_\mu$ |
|---|---|---|---|---|---|---|
| $\rho_\mathrm{e}$ | −0.716 | −0.700 | −0.249 | 0.229 | 0.344 | −0.035 |
| $\xi_\mathrm{e}$ | | 0.592 | 0.251 | −0.337 | −0.307 | −0.006 |
| $(\xi\delta)_\mathrm{e}$ | | | 0.321 | −0.289 | −0.442 | 0.037 |
| $\rho_\mu$ | | | | −0.427 | −0.590 | 0.461 |
| $\xi_\mu$ | | | | | 0.271 | 0.132 |
| $(\xi\delta)_\mu$ | | | | | | −0.116 |

## 4 Results

The result of the most general global fit to single-e, single-$\mu$ and e–$\mu$ correlations with seven free parameters is shown in Table 4. Table 5 gives the individual correlation coefficients. The first errors are due to data and Monte Carlo statistics as obtained from the fit, the second ones are due to systematic uncertainties (see Sect. 4.1). Figures 2 and 3 show the single decay spectra for $\tau \to \mathrm{e}\,\nu_\mathrm{e}\nu_\tau$ and $\tau \to \mu\,\nu_\mu\nu_\tau$ decays, respectively. In both figures, the lightly shaded part of the histogram is the adjusted Monte Carlo prediction using the Michel parameters from the global fit (Table 4).

Note that the fit range for the $\tau \to \mathrm{e}\,\nu_\mathrm{e}\nu_\tau$ spectrum extends from $x = 0$ to 0.9 while for $\tau \to \mu\,\nu_\mu\nu_\tau$ as well as for the e–$\mu$ correlation spectra the full range ($x = 0$ to 1.0) has been used. This is because the background from Bhabha events causes a relatively large systematic uncertainty at high $x$ to single $\tau \to \mathrm{e}\,\nu_\mathrm{e}\nu_\tau$ decays which is no longer present in the correlation spectra where the recoil is required to be a $\tau \to \mu\,\nu_\mu\nu_\tau$ decay. For the $\tau \to \mu\,\nu_\mu\nu_\tau$ single decay (Fig. 3) the $\mathrm{e^+e^-} \to \mu^+\mu^-$ contamination at high $x$ is well simulated and no restriction of the fit range is necessary.

In the plots below the single lepton spectra, the differences between data and Monte Carlo spectra are shown. Since only the shape of the likelihood function is significant and not its scale, there is no absolute criterion for the quality of the fit from the maximum likelihood method itself. As an estimator for the confidence level, the $\chi^2$ prob-

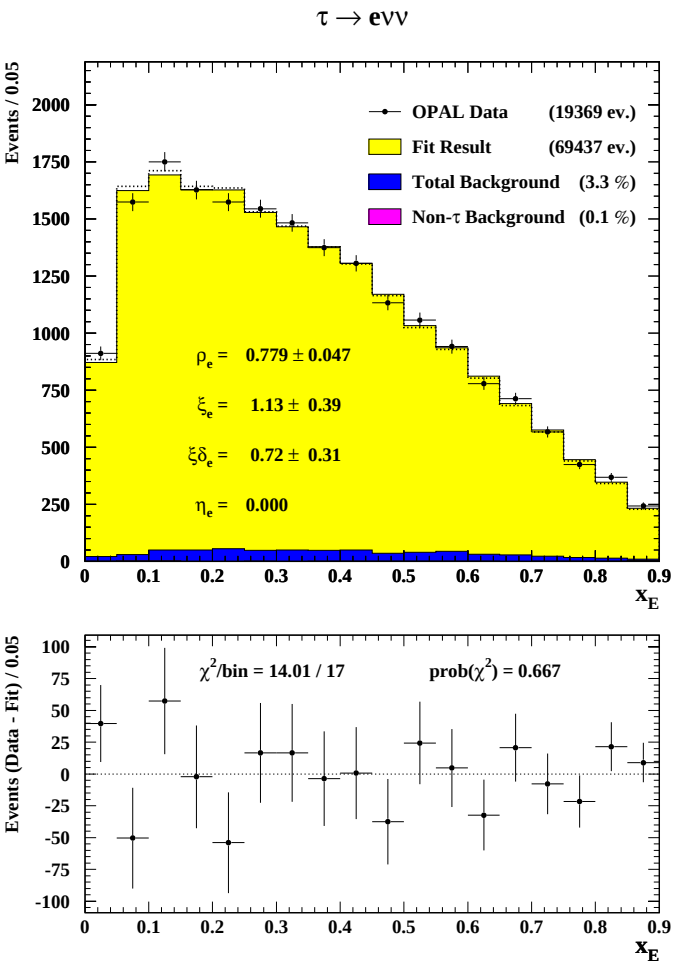


**Fig. 2.** The scaled $\tau \to \mathrm{e}\,\nu_\mathrm{e}\nu_\tau$ electron energy decay spectrum from e–h events. The quoted Michel parameters are the subset from the global fit that determines the plotted electron Monte Carlo spectrum. The dotted line represents the Standard Model expectation

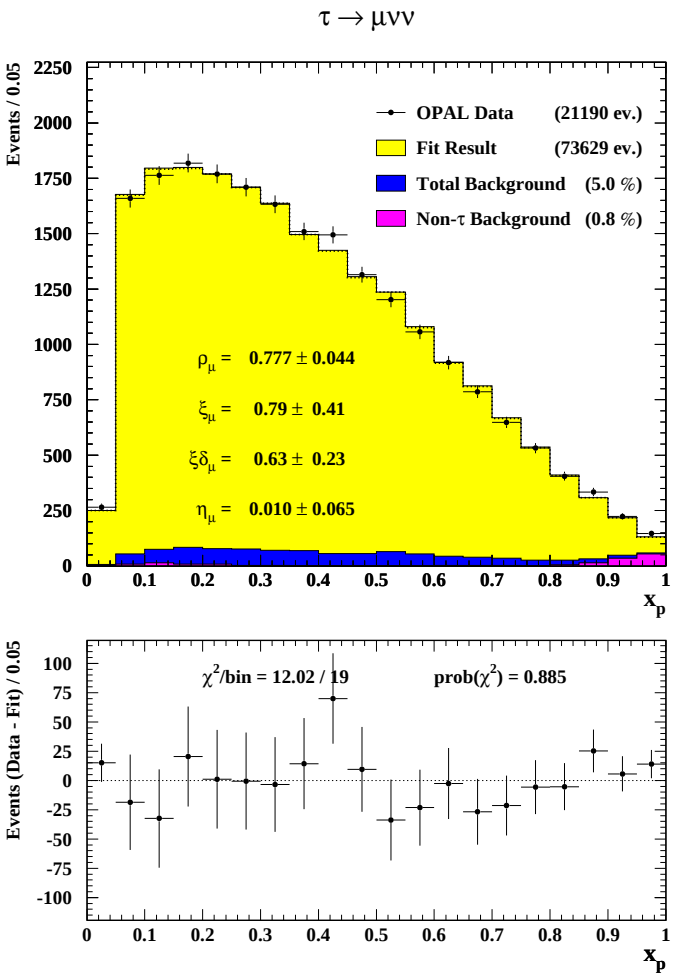


**Fig. 3.** The scaled $\tau \to \mu\,\nu_\mu\nu_\tau$ muon momentum decay spectrum from $\mu$–h events. The quoted Michel parameters are the subset from the global fit that determines the plotted muon Monte Carlo spectrum. The dotted line represents the Standard Model expectation

ability[8] for the plotted bins is appended to Figs. 2 and 3.

Figures 4 and 5 are two different representations of the e–$\mu$ correlation spectrum, displaying slices of $x_\mathrm{e}$ for fixed $x_\mu$ (Fig. 4) and vice versa (Fig. 5). In all figures the dark shaded histogram represents the total background from misidentified $\tau$ decays and the black one the corresponding fraction of $\mathrm{e^+e^-} \to \mathrm{e^+e^-}$ and $\mathrm{e^+e^-} \to \mu^+\mu^-$ events. The background decomposition is listed in Table 3. The fitted Michel parameters of Table 4 are consistent with the V−A prediction of the Standard Model and describe the spectra in Figs. 2–5 well.

[8] It has to be noted that this $\chi^2$ probability is biased towards higher values. Since the number of fit parameters that constrain a specific spectrum cannot be assigned to the different event classes in a unique way the (number of bins minus 1) has been taken as the number of degrees of freedom.

### 4.1 Systematic errors

Various systematic uncertainties arising from different sources, both detector specific and inherent to the method, have been investigated. Besides these systematics, uncertainties concerning the Monte Carlo simulation at the generator level, i.e., radiation effects, branching fractions, process kinematics etc., have been found to be negligible. The Monte Carlo statistical error is already reflected by the fit errors as explained above.

For the study of systematic uncertainties imposed by the Monte Carlo simulation various data control samples have been prepared. Two samples, one of Bhabha and one of $\mu$-pair events, have been selected by using the criteria mentioned in Sect. 2.2. The energy and momentum distributions of these lepton-pair samples show narrow peaks at the beam energy. Two other samples with single lepton cones have been prepared by using a tagging technique. This has been done with preselected two-photon events,

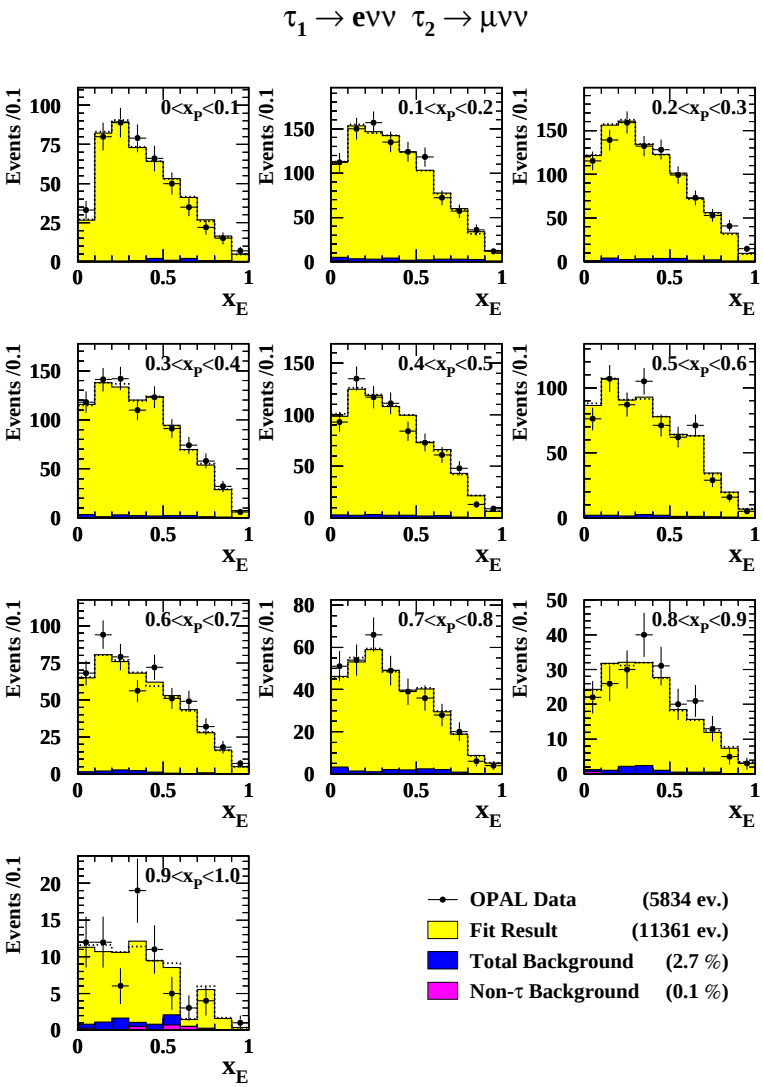


**Fig. 4.** The correlated $\tau \to e\,\nu_e\nu_\tau$ and $\tau \to \mu\,\nu_\mu\nu_\tau$ decay spectra from e–$\mu$ events together with the Monte Carlo distribution from the global fit. The spectrum of the scaled energy, $x_E$, of the decay electron is shown in slices for each bin of the scaled muon momentum, $x_p$. The dotted line represents the Standard Model expectation

**Table 6.** Contributions of systematic uncertainties to the error of each Michel parameter for the global fit. A dash indicates that the listed effect contributes less than 0.001 $(\rho, \eta)$ or 0.01 $(\xi, \xi\delta)$ to the Michel parameter error. Note that the value of $\eta_\mu$ is dominated by the branching ratio constraint

| | $\Delta\rho_e$ | $\Delta\xi_e$ | $\Delta(\xi\delta)_e$ | $\Delta\rho_\mu$ | $\Delta\xi_\mu$ | $\Delta(\xi\delta)_\mu$ | $\Delta\eta_\mu$ |
|---|---|---|---|---|---|---|---|
| Energy scale | 0.017 | 0.11 | 0.11 | – | – | – | – |
| Momentum scale | – | – | – | 0.013 | 0.04 | 0.04 | 0.001 |
| Energy resolution | 0.003 | 0.03 | 0.04 | – | – | – | – |
| Momentum resolution | – | – | – | 0.004 | 0.05 | 0.02 | 0.001 |
| Energy-dependent efficiency | 0.023 | 0.08 | 0.08 | – | – | – | – |
| Momentum-dependent efficiency | – | – | – | 0.009 | 0.07 | 0.01 | – |
| Total | 0.029 | 0.14 | 0.14 | 0.016 | 0.09 | 0.05 | 0.001 |

$\gamma\gamma \to e^+e^-$ and $\gamma\gamma \to \mu^+\mu^-$, where one lepton is tagged based on a clear decay mode identification so that the other cone can be investigated. The same has been done with $e^+e^- \to e^+e^-$ and $e^+e^- \to \mu^+\mu^-$ events.

The following systematic effects, summarized in Table 6, remain. (a) The absolute scale of the energy and momentum measurement of electrons and muons, respectively, has been varied in the Monte Carlo simulation. The scale uncertainty has been determined by comparing $e^+e^- \to e^+e^-$ and $e^+e^- \to \mu^+\mu^-$ events from the data control samples with the corresponding Monte Carlo events. Rescaling the energies and momenta of the Monte Carlo events used in the fit within the observed uncertainty of 0.3% and 0.2%, respectively, results in changes of the Michel parameters as given in Table 6.

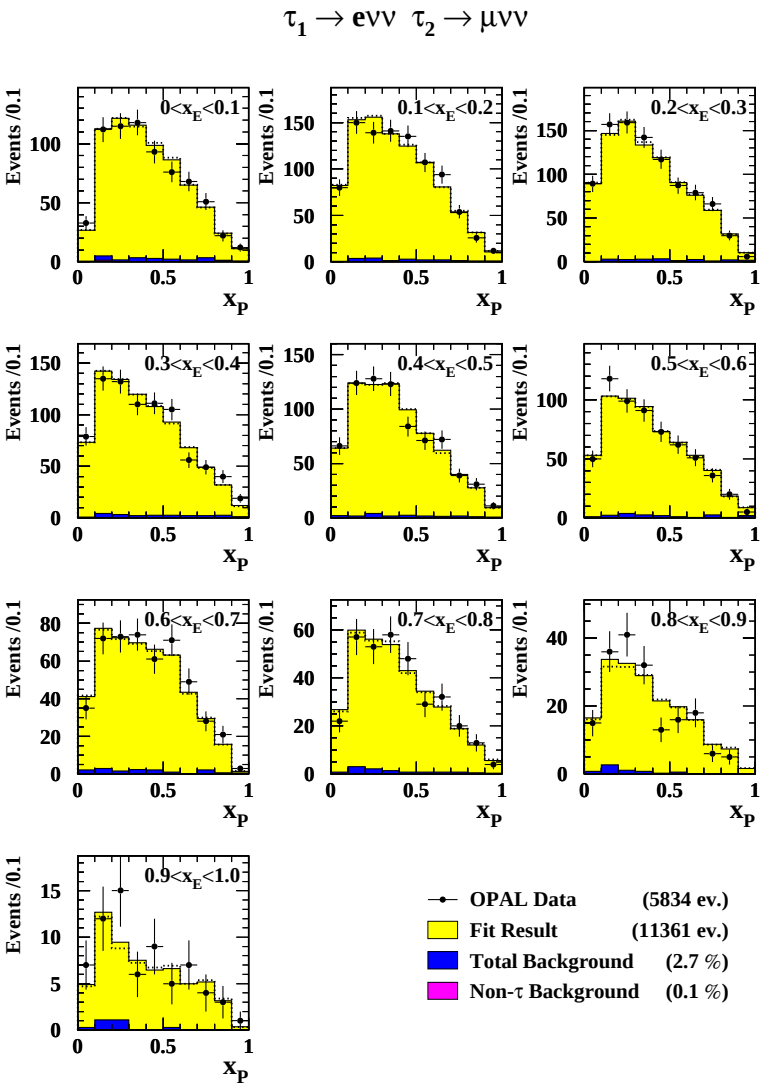


**Fig. 5.** The correlated $\tau \to e\,\nu_e\nu_\tau$ and $\tau \to \mu\,\nu_\mu\nu_\tau$ decay spectra from e–$\mu$ events together with the Monte Carlo distribution from the global fit. The spectrum of the scaled momentum, $x_p$, of the decay muon is shown in slices of each bin of the scaled electron energy, $x_E$. The dotted line represents the Standard Model expectation. (The plots show the same bins as figure 4 in a different order)

(b) The uncertainty in the energy and momentum resolution has been determined from the same control samples which have been used for the previous study. Variation of the resolution leads to the quoted changes.

(c) The efficiency as determined from the Monte Carlo has been compared to the tagged control samples that include Bhabha and $\mu$-pair events covering the high $x$ region as well as two-photon events at low $x$. The events have been used by tagging one lepton while examining the efficiency for identifying the other lepton. The ratio of the efficiencies in data and Monte Carlo samples has been found to be consistent with unity. The uncertainty on this efficiency ratio has been estimated by fitting the low- and the high-$x$ values with a straight line and determining the $1\sigma$ bounds of a possible slope. Since the overall efficiency is not used in the fit only an energy/momentum-dependent discrepancy could possibly affect the result. This has been accounted for by weighting the Monte Carlo events within the uncertainty of the possible slopes.

(d) The background contributions from $\tau$ and non-$\tau$ sources which are estimated from the Monte Carlo simulation have been varied in the fit. Previous studies of the decay mode identification mentioned in Sect. 2.3 showed that the reference distributions of the likelihood variables agree with those of tagged data samples well. Reweighting the Monte Carlo such that it perfectly matches the data causes only slight changes in the resulting purities. The uncertainty of the background is savely estimated to be at the 10% level, with the exception of the Bhabha background which has been varied by a factor of 2. The reason for this is a relatively poor modeling of the Bhabha background especially in the forward region. Due to the small fraction of the background, the variation had no significant impact on the fit result.

(e) The dependence of the fit result on the energy and momentum range has been investigated by omitting the outer bins at low- and high-$x$ values. For the single $\mu$ and the e–$\mu$ spectra the variation of the fit with and without the high-$x$ bins also reflects the sensitivity to the description of the $e^+e^- \to \mu^+\mu^-$ background. No statistically significant change has been observed.

**Table 7.** Result of the e–$\mu$ universality fit

| | $\tau \to \ell\,\nu_\ell\nu_\tau$ |
|---|---|
| $\rho$ | $0.781 \pm 0.028 \pm 0.018$ |
| $\xi$ | $0.98 \pm 0.22 \pm 0.10$ |
| $\xi\delta$ | $0.65 \pm 0.14 \pm 0.07$ |
| $\eta$ | $0.027 \pm 0.055 \pm 0.005$ |

**Table 8.** Correlation coefficients for the e–$\mu$ universality fit

| | $\xi$ | $\xi\delta$ | $\eta$ |
|---|---|---|---|
| $\rho$ | $-0.521$ | $-0.492$ | $0.348$ |
| $\xi$ | | $0.273$ | $-0.022$ |
| $\xi\delta$ | | | $-0.094$ |

(f) Different sets of basis spectra have been used to study the influence of the particular choice of the Michel parameter basis on the description of the data. The same behavior has been observed as for the Monte Carlo study mentioned above with the cross checks of the fitting method. Due to the finite Monte Carlo statistics some bases were less sensitive to the Michel parameters than the preferred one. However, all alternative fits were consistent within their respective fit errors. This means that the basis choice does not contribute to the systematic error.

### 4.2 Lepton universality

With the assumption of universality between electron and muon, i.e., with all couplings $g^\gamma_{\epsilon\omega}$ being the same for $\tau \to \mathrm{e}\,\nu_\mathrm{e}\nu_\tau$ and $\tau \to \mu\,\nu_\mu\nu_\tau$, one set of Michel parameters can be used to describe both leptonic decays. The fit then yields the results in Table 7. The systematic errors have been determined using the same procedure as for the general fit. The correlation coefficients for this fit are listed in Table 8. The results are in agreement with the prediction of a V−A structure of the charged weak current.

### 4.3 Limits on the couplings

From the measurement of the Michel parameters, limits on the absolute values of the couplings $g^\gamma_{\epsilon\omega}$ [see (1)] can be extracted. This is done by constructing positive-semidefinite expressions from the measured parameters. A general approach to find such expressions is to use the boundaries of the physically allowed parameter space as shown in Fig. 6. In three dimensions, the physically allowed region of the three parameters $\rho$, $\xi$ and $\xi\delta$ forms a tetrahedron [46].[9]

An upper bound on $|g^\mathrm{V}_\mathrm{RL}|$ as well as weak upper bounds on $|g^\mathrm{S}_\mathrm{RL}|$ and $|g^\mathrm{T}_\mathrm{RL}|$ can be set from the expression $1-\rho$. Limits on $|g^\mathrm{V}_\mathrm{RR}|$ and $|g^\mathrm{S}_\mathrm{RR}|$ can be retrieved from the expression $\rho - \xi\delta$. Limits on the remaining couplings $|g^\mathrm{S}_\mathrm{LR}|$ and $|g^\mathrm{T}_\mathrm{LR}|$ follow from the probability for the decay of a right-handed $\tau$ lepton which is given below. An even stronger limit on $|g^\mathrm{V}_\mathrm{LR}|$ can be set by regarding a plane in the 3-dimensional parameter space $(\rho, \xi, \xi\delta)$ which yields the expression $1-\rho+\frac{1}{3}\,\xi-\frac{7}{9}\,\xi\delta$. The explicit dependence of these expressions on the couplings is

$$1-\rho = \frac{1}{4}|g^\mathrm{V}_\mathrm{LL}|^2 + |g^\mathrm{V}_\mathrm{LR}|^2 + |g^\mathrm{V}_\mathrm{RL}|^2 + \frac{1}{4}|g^\mathrm{V}_\mathrm{RR}|^2 + \frac{1}{16}|g^\mathrm{S}_\mathrm{LL}|^2 + \frac{1}{16}|g^\mathrm{S}_\mathrm{LR} + 6g^\mathrm{T}_\mathrm{LR}|^2 + \frac{1}{16}|g^\mathrm{S}_\mathrm{RL} + 6g^\mathrm{T}_\mathrm{RL}|^2 + \frac{1}{16}|g^\mathrm{S}_\mathrm{RR}|^2, \quad (26)$$

$$\rho - \xi\delta = \frac{3}{2}|g^\mathrm{V}_\mathrm{RR}|^2 + \frac{3}{8}|g^\mathrm{S}_\mathrm{LR} - 2g^\mathrm{T}_\mathrm{LR}|^2 + \frac{3}{8}|g^\mathrm{S}_\mathrm{RR}|^2, \quad (27)$$

$$1-\rho+\frac{1}{3}\,\xi-\frac{7}{9}\,\xi\delta = |g^\mathrm{V}_\mathrm{LR}|^2 + \frac{1}{4}|g^\mathrm{V}_\mathrm{RR}|^2 + \frac{1}{16}|g^\mathrm{S}_\mathrm{LR} + 6g^\mathrm{T}_\mathrm{LR}|^2 + \frac{1}{16}|g^\mathrm{S}_\mathrm{RR}|^2. \quad (28)$$

Only the coupling $|g^\mathrm{S}_\mathrm{LL}|$ cannot be constrained since it cannot be distinguished from the Standard Model coupling $|g^\mathrm{V}_\mathrm{LL}|$ on basis of the four Michel parameters. An upper bound on $|g^\mathrm{S}_\mathrm{LL}|$ would require the measurement of correlations between one of the neutrinos and the charged lepton [47] or of the cross section for the process $\nu_\tau\ell\to\tau\nu_\ell$[12].

The probability that the $\tau$ lepton decays as a right-handed particle can be calculated as the sum of all couplings of the type $g^\gamma_{\epsilon\mathrm{R}}$ normalized according to (3):

$$Q_\mathrm{R} = \frac{1}{4}|g^\mathrm{S}_\mathrm{LR}|^2 + \frac{1}{4}|g^\mathrm{S}_\mathrm{RR}|^2 + |g^\mathrm{V}_\mathrm{LR}|^2 + |g^\mathrm{V}_\mathrm{RR}|^2 + 3\,|g^\mathrm{T}_\mathrm{LR}|^2 = \frac{1}{2}\left(1+\frac{1}{3}\,\xi-\frac{16}{9}\,\xi\delta\right). \quad (29)$$

Using the correlations between the parameters the e-$\mu$ universality fit yields

$$Q_\mathrm{R} = 0.089 \pm 0.131 < 0.304 \quad (90\%\ \mathrm{C.L.})\ . \quad (30)$$

From the result of the global and of the e–$\mu$ universality fit, respectively, the bounds given in Table 9 can be set at the 90% confidence level. Figure 7 shows the limits on the universal coupling constants normalized to their maximum values ($g^\mathrm{S}_\mathrm{max} = 2$, $g^\mathrm{V}_\mathrm{max} = 1$ and $g^\mathrm{T}_\mathrm{max} = \frac{1}{\sqrt{3}}$) introduced in Sect. 1.1.

### 4.4 Mass of a charged Higgs boson

In models with two scalar field doublets, such as the Minimal Supersymmetric Standard Model (MSSM), the existence of a charged Higgs boson is assumed which contributes to the $\tau$ decay through a scalar coupling. The value of the additional coupling is, assuming vanishing neutrino masses [48–50],

$$g^\mathrm{S}_\ell = -m_\ell\ m_\tau\ \left(\frac{\tan\beta}{m_{\mathrm{H}^\pm}}\right)^2. \quad (31)$$

[9] The three plots in Fig. 6 show the projections of this tetrahedron.

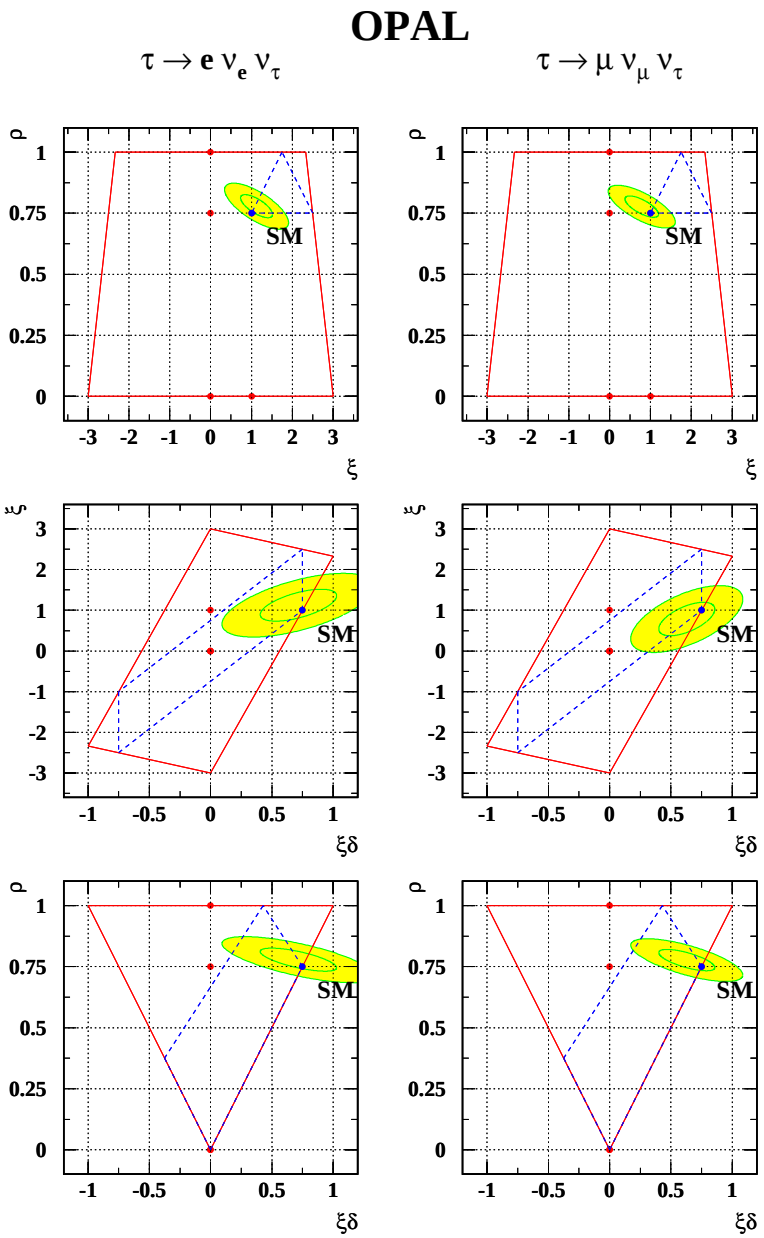


**Fig. 6.** Presentation of the global fit result in 2-dimensional projections of the Michel parameter space. Shown are the 1 and 2 $\sigma$ ellipses of the fitted parameters. The outer (solid) line encloses the physically allowed region of the parameters. The dashed line confines the area that remains when the parameter which is not plotted is fixed to its Standard Model value. The closed circles indicate the basis spectra used in the fit. The labeled one represents the Standard Model

Here $m_{\mathrm{H}^\pm}$ is the mass of the charged Higgs boson, $\tan\beta$ is the ratio of the vacuum expectation values of the two Higgs doublets and $\ell$ denotes either e or $\mu$. Under the assumption that the neutrinos are still left-handed, the couplings are of the type $g^{\mathrm{S}}_{\mathrm{RR}}$. After applying the normalization $N_\ell = |g^{\mathrm{V}}_{\mathrm{LL}}|^2 + \frac{1}{4}|g^{\mathrm{S}}_{\mathrm{RR},\ell}|^2$, the Michel parameters can be written as[10]

$$\rho_\ell = \frac{3}{4} \qquad \xi_\ell = \frac{1-(g^{\mathrm{S}}_{\mathrm{RR},\ell}/2)^2}{1+(g^{\mathrm{S}}_{\mathrm{RR},\ell}/2)^2}\,,$$

$$(\xi\delta)_\ell = \frac{3}{4}\,\xi_\ell\,, \qquad \eta_\ell = -\frac{g^{\mathrm{S}}_{\mathrm{RR},\ell}/2}{1+(g^{\mathrm{S}}_{\mathrm{RR},\ell}/2)^2}\,. \qquad (32)$$

[10] This can be verified by inserting the normalized $g^{\mathrm{V}}_{\mathrm{LL}}$ and $g^{\mathrm{S}}_{\mathrm{RR}}$ into the definition of the Michel parameters given in (8).

By using the above relations, the value of $m_{\mathrm{H}^\pm}/\tan\beta$ can be fitted directly to the data. The likelihood function saturates for high Higgs boson masses or small values of $\tan\beta$. From the log likelihood a limit can be extracted as[11]

$$m_{H^\pm} > 0.97 \times \tan\beta \ \text{GeV} \quad (95\%\ \text{C.L.}). \qquad (33)$$

It should be noted that this limit can be improved by using world averages as input for the constraint on the $\eta$ parameter.

[11] The following limits are determined as the value at which the log likelihood has dropped by the amount that corresponds to the quoted confidence level.

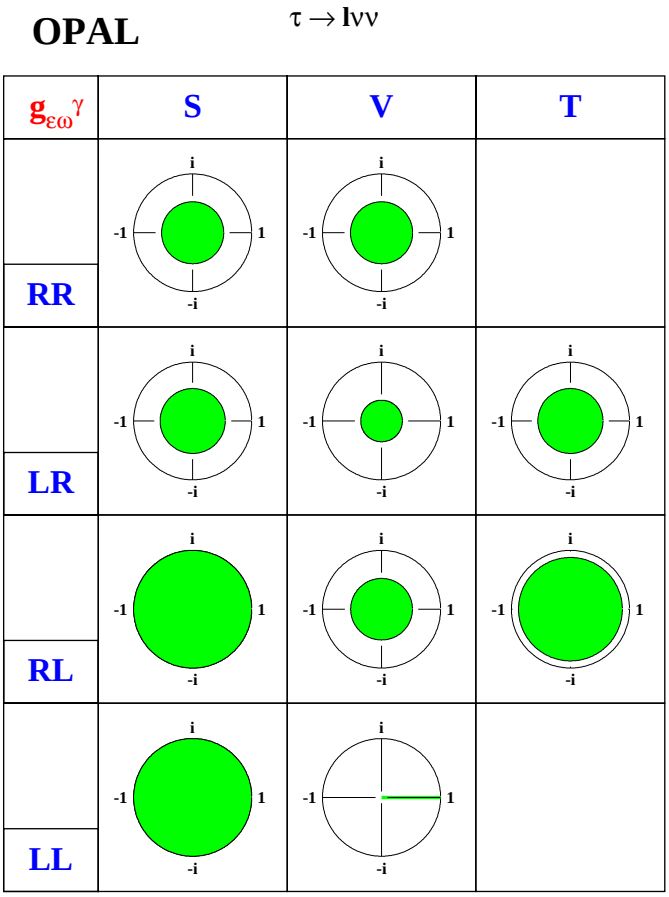


**Fig. 7.** 90% confidence limits on the normalized coupling constants $g^{\gamma}_{\epsilon\omega}/g^{\gamma}_{\max}$ (with $g^{\mathrm{S}}_{\max}=2$, $g^{\mathrm{V}}_{\max}=1$ and $g^{\mathrm{T}}_{\max}=1/\sqrt{3}$) under assumption of e–$\mu$ universality. The Standard Model coupling $g^{\mathrm{V}}_{\mathrm{LL}}$ which is not constrained is chosen to be real and positive

### 4.5 Left–right symmetric model

In left–right symmetric models, parity violation of the charged current is caused by spontaneous symmetry breaking. In such models a second W boson is assumed [51,52]. The mass eigenstates $\mathrm{W}_{1,2}$ are not necessarily identical to the weak eigenstates $\mathrm{W}_{\mathrm{L,R}}$ as mixing can occur. The model is parameterized by the mass ratio $\beta$ of the physical eigenstates,

$$\beta = \frac{m^2_{\mathrm{W}_1}}{m^2_{\mathrm{W}_2}}, \tag{34}$$

and by the mixing angle $\zeta$ that connects the physical masses to the masses of the weak eigenstates,

$$m^2_{\mathrm{W}_{1,2}} = \frac{1}{2}\left(m^2_{\mathrm{W_L}} + m^2_{\mathrm{W_R}} \pm \frac{m^2_{\mathrm{W_L}} - m^2_{\mathrm{W_R}}}{\cos 2\zeta}\right). \tag{35}$$

In this model the Michel parameters can be written as

$$\rho = \frac{3}{4}\cos^4\zeta\left(1+\tan^4\zeta + \frac{4\beta}{1+\beta^2}\tan^2\zeta\right),$$

**Table 9.** 90% confidence limits on the coupling constants for the global fit and under the assumption of e–$\mu$ universality. As mentioned in the text, no limits can be set on the couplings $g^{\mathrm{S}}_{\mathrm{LL}}$ and $g^{\mathrm{V}}_{\mathrm{LL}}$ which are listed only for completeness

| | $\tau \to \mathrm{e}\,\nu_{\mathrm{e}}\nu_\tau$ | $\tau \to \mu\,\nu_\mu\nu_\tau$ | $\tau \to \ell\,\nu_\ell\nu_\tau$ |
|---|---|---|---|
| $\lvert g^{\mathrm{S}}_{\mathrm{RR}}\rvert$ | $< 1.36$ | $< 1.25$ | $< 1.05$ |
| $\lvert g^{\mathrm{S}}_{\mathrm{LR}}\rvert$ | $< 1.40$ | $< 1.27$ | $< 1.10$ |
| $\lvert g^{\mathrm{S}}_{\mathrm{RL}}\rvert$ | $< 2.00$ | $< 2.00$ | $< 2.00$ |
| $\lvert g^{\mathrm{S}}_{\mathrm{LL}}\rvert$ | $\leq 2$ | $\leq 2$ | $\leq 2$ |
| $\lvert g^{\mathrm{V}}_{\mathrm{RR}}\rvert$ | $< 0.68$ | $< 0.62$ | $< 0.53$ |
| $\lvert g^{\mathrm{V}}_{\mathrm{LR}}\rvert$ | $< 0.43$ | $< 0.39$ | $< 0.35$ |
| $\lvert g^{\mathrm{V}}_{\mathrm{RL}}\rvert$ | $< 0.56$ | $< 0.55$ | $< 0.52$ |
| $\lvert g^{\mathrm{V}}_{\mathrm{LL}}\rvert$ | $\leq 1$ | $\leq 1$ | $\leq 1$ |
| $\lvert g^{\mathrm{T}}_{\mathrm{LR}}\rvert$ | $< 0.41$ | $< 0.37$ | $< 0.32$ |
| $\lvert g^{\mathrm{T}}_{\mathrm{RL}}\rvert$ | $< 0.52$ | $< 0.52$ | $< 0.51$ |

$$\xi = \cos^2\zeta\left(1-\tan^2\zeta\right)\frac{1-\beta^2}{1+\beta^2}, \tag{36}$$

$$\xi\delta = \frac{3}{4}\xi,$$

$$\eta = 0.$$

A limit on $\beta$ can be transformed into a limit on $m_{\mathrm{W}_2}$ by using the direct measurement of the W mass: $m_{\mathrm{W}_1} = (80.43 \pm 0.08)\,\mathrm{GeV}$ [20].

For arbitrary mixing the upper plot of Fig. 8 shows the one, two and three $\sigma$ contours of the log likelihood as a function of $\beta$ and $\zeta$. Integration of the two-dimensional likelihood over $\zeta$ yields the corresponding function shown in in the lower left plot of the same figure. From this likelihood a limit on $m_{\mathrm{W}_2}$ which is valid for arbitrary mixing can be extracted as

$$m_{\mathrm{W}_2} > 137\,\mathrm{GeV} \quad (95\%\ \mathrm{C.L.}). \tag{37}$$

Similarly, integration over $m_{\mathrm{W}_2}$ allows one to set bounds on the mixing angle independently of the $\mathrm{W}_2$ mass (lower right plot):

$$|\zeta| < 0.12 \quad (95\%\ \mathrm{C.L.}). \tag{38}$$

For $\zeta = 0$, $\mathrm{W}_2$ and $\mathrm{W_R}$ become identical, and a limit on $m_{\mathrm{W_R}}$ can be given from a fit of the Michel parameter $\xi$ alone. In this case there is no mixing but an additional coupling to a pure right-handed W that is proportional to its inverse mass:[12]

$$g^{\mathrm{V}}_{\mathrm{LL,RR}} \sim \frac{1}{m_{\mathrm{W_{L,R}}}}. \tag{39}$$

Under the assumption of no mixing the following limit is extracted from the log likelihood function:

$$m_{\mathrm{W_R}} > 145\,\mathrm{GeV} \quad (95\%\ \mathrm{C.L.}). \tag{40}$$

[12] Inserting the normalized $g^{\mathrm{V}}_{\mathrm{LL}}$ and $g^{\mathrm{V}}_{\mathrm{RR}}$ into the definition of the Michel parameters (8) yields the above relations for $\zeta = 0$.

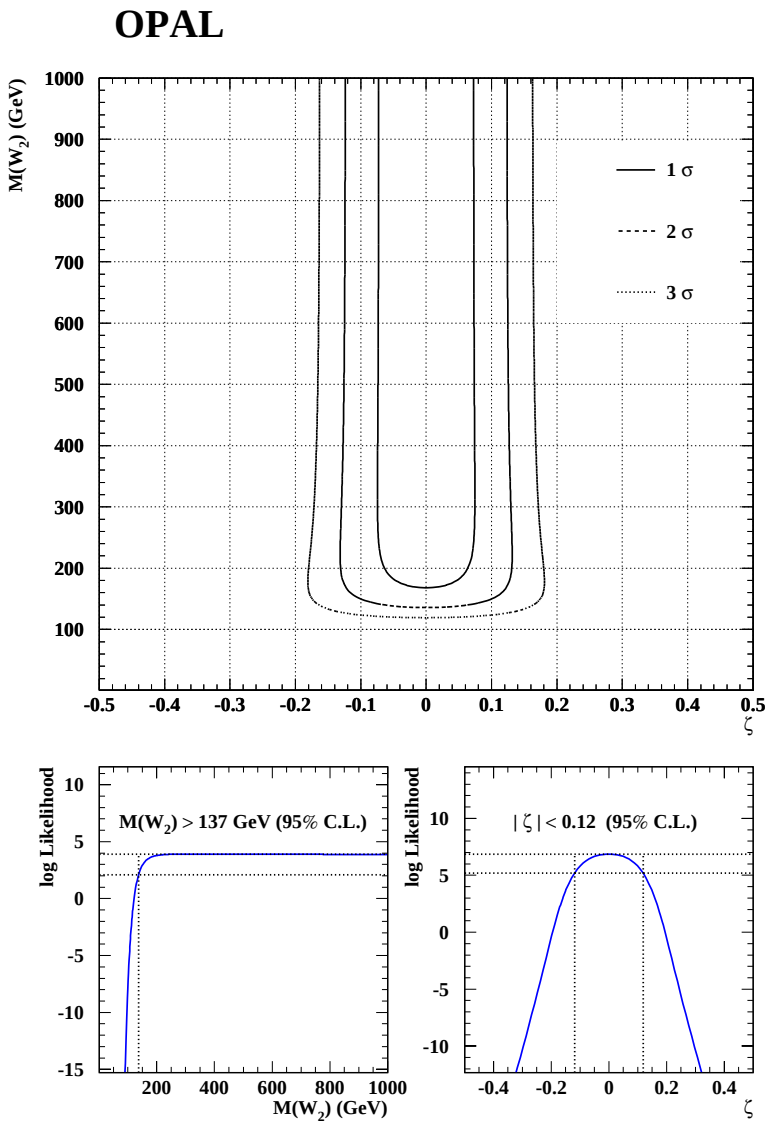


**Fig. 8.** Log likelihood as a function of the mass of a second W boson, $m_{\mathrm{W}_2}$, and the mixing angle $\zeta$ in the left–right symmetric model (upper plot). From this likelihood function limits on $m_{\mathrm{W}_2}$ (lower left plot) and $\zeta$ (lower right plot) are calculated after integration of the likelihood over the second variable

## 5 Summary

The Michel parameters of the leptonic $\tau$ decays have been measured from the data collected with the OPAL detector in the years 1990 to 1995. The parameters $\rho_\ell$, $\xi_\ell$, $(\xi\delta)_\ell$ and $\eta_\mu$ (with $\ell = \mathrm{e}, \mu$) were extracted from the energy spectra of the charged decay leptons and from their energy–energy correlations. A new method has been presented which involves a global likelihood fit of Monte Carlo generated events with radiative corrections at the generator level and complete detector simulation and background treatment. In the framework of the most general Lorentz structure for both leptonic decays the result of the global fit is

$$\begin{aligned}
\rho_{\mathrm{e}} &= 0.779 \pm 0.047 \pm 0.029,\\
\rho_{\mu} &= 0.777 \pm 0.044 \pm 0.016,\\
\xi_{\mathrm{e}} &= 1.13 \pm 0.39 \pm 0.14,\\
\xi_{\mu} &= 0.79 \pm 0.41 \pm 0.09,\\
(\xi\delta)_{\mathrm{e}} &= 0.72 \pm 0.31 \pm 0.14,\\
(\xi\delta)_{\mu} &= 0.63 \pm 0.23 \pm 0.05,\\
\eta_{\mu} &= 0.010 \pm 0.065 \pm 0.001,
\end{aligned}$$

where the value of $\eta$ is dominated by a constraint using the previously published values of the leptonic branching ratios and the $\tau$ lifetime. The $\tau$ polarization has been inferred from neutral current data. The Michel parameters have also been measured under the assumption of e–$\mu$ universality and in terms of specific models. The e–$\mu$ universality fit yields

$$\begin{aligned}
\rho &= 0.781 \pm 0.028 \pm 0.018,\\
\xi &= 0.98 \pm 0.22 \pm 0.10,\\
\eta &= 0.027 \pm 0.055 \pm 0.005,\\
\xi\delta &= 0.65 \pm 0.14 \pm 0.07.
\end{aligned}$$

Limits have been obtained on the individual coupling constants as well as on the masses of new intermediate bosons, such as a right-handed W boson, $\mathrm{W_R}$, and a charged Higgs boson. No indication for new physics processes has been observed. The results are in agreement with the V−A prediction of the Standard Model.

**Table 10.** Example coupling constants and corresponding Michel parameters

| Type of interaction | Coupling constants | Michel parameters | | | |
|---|---|---|---|---|---|
| $\ell$-$\nu_\ell$vertex $\otimes$ $\tau$-$\nu_\tau$vertex | | $\rho$ | $\xi$ | $\xi\delta$ | $\eta$ |
| V−A $\otimes$ V−A | $g^{\rm V}_{\rm LL} = 1$ | 3/4 | 1 | 3/4 | 0 |
| V+A $\otimes$ V+A | $g^{\rm V}_{\rm RR} = 1$ | 3/4 | −1 | −3/4 | 0 |
| V $\otimes$ V | $g^{\rm V}_{\rm LL} = g^{\rm V}_{\rm RL} = g^{\rm V}_{\rm LR} = g^{\rm V}_{\rm RR} = 1/2$ | 3/8 | 0 | 0 | 0 |
| A $\otimes$ A | $g^{\rm V}_{\rm LL} = -g^{\rm V}_{\rm RL} = -g^{\rm V}_{\rm LR} = g^{\rm V}_{\rm RR} = 1/2$ | 3/8 | 0 | 0 | 0 |
| V−A $\otimes$ V+A | $g^{\rm V}_{\rm LR} = 1$ | 0 | 3 | 0 | 0 |
| V+A $\otimes$ V−A | $g^{\rm V}_{\rm RL} = 1$ | 0 | −3 | 0 | 0 |
| S+P $\otimes$ S−P | $g^{\rm S}_{\rm LL} = 2$ | 3/4 | 1 | 3/4 | 0 |
| S−P $\otimes$ S+P | $g^{\rm S}_{\rm RR} = 2$ | 3/4 | −1 | −3/4 | 0 |
| S $\otimes$ S | $g^{\rm S}_{\rm LL} = g^{\rm S}_{\rm RL} = g^{\rm S}_{\rm LR} = g^{\rm S}_{\rm RR} = 1$ | 3/4 | 0 | 0 | 0 |
| P $\otimes$ P | $-g^{\rm S}_{\rm LL} = g^{\rm S}_{\rm RL} = g^{\rm S}_{\rm LR} = -g^{\rm S}_{\rm RR} = 1$ | 3/4 | 0 | 0 | 0 |
| S+P $\otimes$ S+P | $g^{\rm S}_{\rm LR} = 2$ | 3/4 | −1 | −3/4 | 0 |
| S−P $\otimes$ S−P | $g^{\rm S}_{\rm RL} = 2$ | 3/4 | 1 | 3/4 | 0 |
| T $\otimes$ T | $g^{\rm T}_{\rm LR} = g^{\rm T}_{\rm RL} = \sqrt{1/6}$ | 1/4 | 0 | 0 | 0 |
| 50% V−A $\otimes$ V−A, 50% S $\otimes$ S | $g^{\rm V}_{\rm LL} = g^{\rm S} = \sqrt{1/2}$ | 3/4 | 1/2 | 3/8 | 1/4 |
| 50% V−A $\otimes$ V−A, 50% S−P $\otimes$ S+P | $g^{\rm V}_{\rm LL} = \sqrt{1/2},\ g^{\rm S}_{\rm RR} = \sqrt{2}$ | 3/4 | 1 | 0 | 1/2 |
| 50% V∓A $\otimes$ V∓A, 50% S±P $\otimes$ S∓P | $g^{\rm V}_{\rm LL} = g^{\rm V}_{\rm RR} = 1/2,\ g^{\rm S}_{\rm RR} = g^{\rm S}_{\rm LL} = 1$ | 3/4 | 0 | 0 | 1/2 |
| 50% V−A $\otimes$ V−A, 50% V+A $\otimes$ V−A | $g^{\rm V}_{\rm LL} = g^{\rm V}_{\rm RL} = \sqrt{1/2}$ | 3/8 | −1 | 3/8 | 0 |
| 50% V+A $\otimes$ V+A, 50% V−A $\otimes$ V+A | $g^{\rm V}_{\rm RR} = g^{\rm V}_{\rm LR} = \sqrt{1/2}$ | 3/8 | 1 | −3/8 | 0 |
| 50% V−A $\otimes$ V+A, 50% V+A $\otimes$ V−A | $g^{\rm V}_{\rm LR} = g^{\rm V}_{\rm RL} = \sqrt{1/2}$ | 0 | 0 | 0 | 0 |
| 67% V−A $\otimes$ V+A, 33% V+A $\otimes$ V−A | $g^{\rm V}_{\rm LR} = \sqrt{2/3},\ g^{\rm V}_{\rm RL} = \sqrt{1/3}$ | 0 | 1 | 0 | 0 |
| 75% S±P $\otimes$ S±P, 25% T $\otimes$ T | $g^{\rm S}_{\rm LR} = g^{\rm S}_{\rm RL} = \sqrt{3/2},\ g^{\rm T} = -\sqrt{1/24}$ | 1 | 0 | 0 | 0 |
| 12.5% S±P $\otimes$ S±P, 50% V∓A $\otimes$ V±A, 37.5% T $\otimes$ T | $g^{\rm S}_{\rm LR} = g^{\rm S}_{\rm RL} = g^{\rm V}_{\rm LR} = g^{\rm V}_{\rm RL} = 1/2,\ g^{\rm T} = 1/4$ | 0 | 0 | 0 | 1 |

*Acknowledgements.* We particularly wish to thank the SL Division for the efficient operation of the LEP accelerator at all energies and for their continuing close cooperation with our experimental group. We thank our colleagues from CEA, DAPNIA/SPP, CE-Saclay for their efforts over the years on the time-of-flight and trigger systems which we continue to use. In addition to the support staff at our own institutions we are pleased to acknowledge the: Department of Energy, USA; National Science Foundation, USA; Particle Physics and Astronomy Research Council, UK; Natural Sciences and Engineering Research Council, Canada; Israel Science Foundation, administered by the Israel Academy of Science and Humanities; Minerva Gesellschaft; Benoziyo Center for High Energy Physics; Japanese Ministry of Education, Science and Culture (the Monbusho) and a grant under the Monbusho International Science Research Program; German Israeli Bi-national Science Foundation (GIF); Bundesministerium für Bildung, Wissenschaft, Forschung und Technologie, Germany; National Research Council of Canada; Research Corporation, USA; Hungarian Foundation for Scientific Research, OTKA T-016660, T023793 and OTKA F-023259.

## References

1. ALEPH, D. Buskulic et al., Phys. Lett. B **346**, 379 (1995)
2. L3, M. Acciarri et al., Phys. Lett. B **377**, 313 (1996)
3. ARGUS, H. Albrecht et al., Phys. Lett. B **246**, 278 (1990)
4. ARGUS, H. Albrecht et al., Phys. Lett. B **316**, 608 (1993)
5. ARGUS, H. Albrecht et al., Phys. Lett. B **341**, 441 (1995)
6. ARGUS, H. Albrecht et al., Phys. Lett. B **349**, 576 (1995)
7. ARGUS, H. Albrecht et al., (1997), hep-ex/9711022
8. SLD, K. Abe et al., Phys. Rev. Lett. **78**, 4691 (1997)
9. CLEO, R. Ammar et al., Phys. Rev. Lett. **78**, 4686 (1997)
10. CLEO, J. P. Alexander et al., Phys. Rev. D **56**, 5320 (1997)
11. Crystal Ball, H. Janssen et al., Phys. Lett. B **228**, 273 (1989)
12. W. Fetscher, H. J. Gerber, K. F. Johnson, Phys. Lett. B **173**, 102 (1986)
13. A. Pich, J. P. Silva, Phys. Rev. D **52**, 4006 (1995)
14. F. Scheck, Phys. Rept. **44**, 187 (1978)
15. L. Michel, Proc. Phys. Soc. A **63**, 514 (1950)
16. C. Bouchiat, L. Michel, Phys. Rev. **106**, 170 (1957)
17. C. A. Nelson, Phys. Rev. D **40**, 123 (1989)
18. W. Fetscher, Phys. Rev. D **42**, 1544 (1990)
19. D. Bardin et al., CERN Report No. TH 6443/92, 1992 (unpublished)
20. D. Abbaneo et al., CERN Report No. PPE-97-154, 1997 (unpublished)
21. OPAL, G. Alexander et al., Z. Phys. C **72**, 365 (1996)
22. OPAL, K. Ahmet et al., Nucl. Instrum. Meth. A **305**, 275 (1991)
23. OPAL, A. Honma, Nucl. Instrum. Meth. A **348**, 409 (1994)
24. OPAL, R. Akers et al., Z. Phys. C **65**, 1 (1995)
25. OPAL, G. Alexander et al., Phys. Lett. B **266**, 201 (1991)
26. OPAL, R. Akers et al., Z. Phys. C **66**, 31 (1995)
27. S. Jadach, B. F. L. Ward, Z. Wąs, Comput. Phys. Commun. **66**, 276 (1991)

28. S. Jadach, J. H. Kühn, Z. Wąs, Comput. Phys. Commun. **64**, 275 (1991)
29. M. Schmidtler, Karlsruhe U., IEKP Report No. KA-93-14, 1993 (unpublished)
30. S. Jadach, M. Jezabek, J. H. Kühn, Z. Wąs, Comput. Phys. Commun. **70**, 69 (1992)
31. R. Decker, S. Jadach, J. H. Kühn, Z. Wąs, Comput. Phys. Commun. **76**, 361 (1993)
32. E. Barberio, B. van Eijk, Z. Wąs, Comput. Phys. Commun. **66**, 115 (1991)
33. M. Bohm, A. Denner, W. Hollik, Nucl. Phys. B **304**, 687 (1988)
34. F. A. Beerends, R. Kleiss, W. Hollik, Nucl. Phys. B **304**, 712 (1988)
35. S. Jadach, B. F. L. Ward, Z. Wąs, Comput. Phys. Commun. **79**, 503 (1994)
36. R. Battacharya, J. Smith, G. Grammer, Phys. Rev. D **15**, 3267 (1977)
37. J. Smith, J. A. M. Vermaseren, G. Grammer, Phys. Rev. D **15**, 3280 (1977)
38. OPAL, J. Allison et al., Nucl. Instrum. Meth. A **317**, 47 (1992)
39. R. Brun, F. Bruyant, M. Maire, A. C. McPherson, P. Zanarini, CERN Report No. DD/EE/84-1, 1987 (unpublished)
40. F. James, M. Roos, Comput. Phys. Commun. **10**, 343 (1975)
41. R. Barlow, C. Beeston, Comput. Phys. Commun. **77**, 219 (1993)
42. A. Stahl, Phys. Lett. B **324**, 121 (1994)
43. W. J. Marciano, A. Sirlin, Phys. Rev. Lett. **61**, 1815 (1988)
44. OPAL, G. Alexander et al., Phys. Lett. B **374**, 341 (1996)
45. OPAL, R. Akers et al., Z. Phys. C **66**, 543 (1995)
46. A. Rougé, Ecole Polytechnique Report No. X-LPNHE-95-01, 1995 (unpublished)
47. C. Jarlskog, Nucl. Phys. **75**, 659 (1966)
48. H. E. Haber, SLAC Report No. SLAC-0343, 1989 (unpublished)
49. W. Hollik, T. Sack, Phys. Lett. B **284**, 427 (1992)
50. B. McWilliams, L.-F. Li, Nucl. Phys. B **179**, 62 (1981)
51. J. Polak, M. Zralek, Nucl. Phys. B **363**, 385 (1991)
52. J. Polak, M. Zralek, Phys. Rev. D **46**, 3871 (1992)